

MID-IR AND CO OBSERVATIONS OF THE IR/X-RAY LUMINOUS SEYFERT I GALAXY
NGC 985: THE MAKING OR BREAKING OF A ULIRG?P. N. APPLETON¹Department of Physics and Astronomy, Iowa State University, Ames, IA 50011
apple@ipac.caltech.edu

V. CHARMANDARIS

Astronomy Department, Cornell University, 106 Space Sciences Bldg, Ithaca NY 14853
vassilis@astro.cornell.edu

YU GAO

Infrared Processing and Analysis Center, MS 100-22, California Institute of Technology, Pasadena CA 91125
gao@ipac.caltech.edu

F. COMBES

Observatoire de Paris, DEMIRM, 61 Ave de l'Observatoire, F-75014 Paris, France
francoise.combes@obspm.fr

F. GHIGO

NRAO, P. O. Box 2, Green Bank, West Virginia WV 24944
fghigo@gb.nrao.edu

C. HORELLOU

Onsala Space Observatory, Centre for Astrophysics & Space Science, Chalmers University of Technology,
S-43992 Onsala, Sweden
horellou@oso.chalmers.se

I. F. MIRABEL

CEA/DSM/DAPNIA Service d'Astrophysique, F-91191 Gif-sur-Yvette, France
& Instituto de Astronomía y Física del Espacio, Conicet, Argentina
mirabel@discovery.saclay.cea.fr*ApJ Accepted September 24 2001*

ABSTRACT

We describe ISO^a and BIMA observations of the $z = 0.04$ Seyfert 1 ring galaxy NGC 985 which suggest close parallels with some quasar host galaxies. NGC 985 contains two closely spaced nuclei embedded in an $R^{1/4}$ -law stellar bulge and an outer ring, evidence of an ongoing merger. The system contains $\sim 1.8 \times 10^{10} M_{\odot}$ of highly disturbed molecular gas which lies in an asymmetric bar-like structure with the peak in observed CO column densities significantly offset from the compact double nucleus. In contrast to this, the ISO observations show strong dust emission centered on the AGN, located in one of the two nuclei. Fainter CO, MIR, and radio continuum emission provide a glimpse of the complexities of star formation in the outer ring.

An analysis of the kinematics of the main CO emission reveal evidence for two dynamically distinct molecular components within NGC 985. The first is a set of isolated super-giant molecular clouds (SGMCs) which are concentrated within 9–10 kpc of the active nucleus. Although randomly distributed about the center, the clouds may form part of a clumpy highly-disturbed disk which may be either just forming around double-nucleus (the making of a ULIRG), or alternatively may be in the process of being disrupted-perhaps as a result of a powerful nuclear outflow (the breaking of a ULIRG). A second major concentration of CO lies offset from the double-nucleus in a dynamically coherent ridge of emission in which powerful star formation is occurring. We tentatively associate CO emission with two out of six UV absorption-lines seen in the blue wing of the very broad Ly α emission. Such an association would imply a complex inter-relationship between the nuclear CO cloud population in colliding systems, and AGN-driven winds.

^a ISO was an ESA project with instruments funded by ESA Member States (especially the PI countries: France, Germany, the Netherlands and the United Kingdom) with the participation of ISAS and NASA.

Subject headings: infrared: galaxies — galaxies: individual (NGC 985) — galaxies: interactions — galaxies: Seyfert — galaxies: starburst — quasars: absorption lines

1. INTRODUCTION

The detection of large quantities of molecular gas in the host galaxies of quasars (e.g. Scoville et al. 1993; Schinnerer et al. 1998; Guilloateau et al. 1999; Evans et al. 2001; Papadopoulos et al. 2001) lends strong support to the

idea that quasars and molecular-rich Ultraluminous Infrared Galaxies (ULIRGs) may be related in evolutionary terms – an idea first suggested on the basis of their similar far-infrared (FIR) properties and comparable space densities (Soifer et al. 1986; Sanders et al. 1988; Evans et al. 1999). Such ideas find support in the HST imag-

¹ Now at SIRTf Science Center, California Institute of Technology, Mailcode 249-6, 1200 E. California Av., Pasadena, CA 91125

ing of nearby quasars, which show that some quasar host galaxies have disturbed morphologies, and are sometimes “caught in the act” of merging (e.g. Bahcall et al. 1995, 1997). Given the potential importance of the molecular gas (either for quasar fueling, or for the initiation of major star formation activity in the host), we are investigating some nearby examples of galaxies which share some molecular and morphological similarities to host quasars, but are close enough that detailed observations can be made.

NGC 985 (Mrk 1048, VV 285) is a peculiar galaxy which was first observed spectroscopically by de Vaucouleurs & de Vaucouleurs (1975), and contains a Seyfert 1 nucleus in the southern part of the ring. Very broad hydrogen and He I $\lambda 5876$ lines in excess of $13,000 \text{ km s}^{-1}$ are seen in the nucleus, along with other indications of high excitation suggesting the existence of an optically-thick accretion disk (Stanga et al. 1991). The nucleus lies at the center of a large IR-bright bulge. Observations at optical and near-IR wavelengths have demonstrated that this nucleus is double (Rodríguez Espinosa & Stanga 1990; Appleton & Marcum 1993; Pérez García & Rodríguez Espinosa 1996, – see also archival HST WFPC and NICMOS images) with a separation of only 3 arcsecs (~ 2.5 kpc). This strongly suggests that the galaxy is undergoing a merger in which the nucleus of the intruder galaxy responsible for the ring formation is already sinking towards the core of the primary galaxy (Pérez García & Rodríguez Espinosa 1996). The one-armed spiral/ring, and the offset nature of the nucleus that dominates the luminosity from the radio through to the X-rays, suggest some similarities with some recently imaged quasar hosts galaxies. In particular, the quasars PKS 2349-014 and PKS 0316-346 (Bahcall et al. 1995, 1997), have very similar morphologies to NGC 985, containing highly offset nuclei and outer ring loops. Although milder examples of offset nuclei are common in samples of collisional ring galaxies, offsets as extreme as the one in NGC 985 are very rare (see Appleton & Struck-Marcell 1996, for a review).

NGC 985 has an IR luminosity of $L_{\text{IR}} = 1.8 \times 10^{11} L_{\odot}$, which is the largest in a sample of ring galaxies observed by IRAS (Appleton & Struck-Marcell 1987), placing it in the category of LIRGs (Sanders & Mirabel 1996). The absolute magnitude of NGC 985 ($M_V = -22.58$ from Appleton & Marston 1997) places it in a similar range of luminosities to that of radio-loud quasar hosts (Bahcall et al. 1997), despite the fact that NGC 985 contains a radio source of only a few mJy (this paper – see also Ulvestad & Wilson 1984). NGC 985 is a powerful X-ray source (Brandt et al. 1994) with a spectrum which is consistent with both a hard power-law component and a substantial soft component. The X-ray spectrum is best fitted if an additional warm-absorber is placed along the line of sight to the AGN.

Recent HST STIS observations (S. Penton & J. Stocke, U. of Colorado: Private Communication) also indicate the presence of at least 6 separate narrow UV absorption lines in the blue wing of the broad $\text{Ly}\alpha$ emission line. We will argue in this paper that two of these lines may have CO emission counterparts, suggesting a possible interaction between a nuclear AGN-driven outflow and the molecular gas.

The primary nucleus (hereafter N1—following the terminology of Pérez García & Rodríguez Espinosa 1996) of NGC 985 has a systemic velocity of $12,814 \pm 15 \text{ km s}^{-1}$ ($z = 0.04$) based on absorption-line studies performed by Arribas et al. (1999). The secondary nucleus (N2) has a systemic velocity of $13,096 \pm 15 \text{ km s}^{-1}$. Assuming a Hubble constant of $75 \text{ km s}^{-1} \text{ Mpc}^{-1}$, we adopt throughout this paper a distance to NGC 985 of 170 Mpc, so in our figures an angular distance of 10 arcsec corresponds to a projected distance of ~ 8 kpc.

Details on our observations are presented in Section 2 and the main imaging results are shown in Section 3. In Sections 4 and 5 we elaborate on the kinematics and dynamics of the galaxy based on the CO, while in Sections 6 and 7 we present the MIR evidence for peculiarities in the star formation properties of the nucleus. In Section 8 we discuss the physical conditions in the outer ring H II regions, and in Section 9 we explore a potential link with of the observed UV absorption lines. In Section 10 we discuss the current and future evolution of NGC 985, and our conclusions are presented in Section 11.

2. OBSERVATIONS

2.1. Space-based Mid-IR Observations

NGC 985 was observed by ISOCAM, a 32×32 pixel array on board the ISO satellite (Cesarsky et al. 1996; Kessler et al. 1996) on December 31 1997 (ISO revolution 776) as part of an ISO-GO observation of bright northern ring galaxies (see also Charmandaris et al. 1999; Appleton et al. 1999, 2000; Charmandaris et al. 2001). The galaxy was imaged through 4 filters, LW1 (4.5 [4.0-5.0] μm), LW7 (9.62 [8.5-10.7] μm), LW8 (11.4 [10.7-12.0] μm), and LW3 (15.0 [12.0-18.0] μm) with on-source time of ~ 10 minutes per filter.

A lens resulting in a 3 arcsec pixel field of view, was used to create a 3×3 raster map in a “microscan” mode in both directions (the telescope was moved 4 arcsecs between each element of the raster in a regular pattern), and the full width at half maximum of the point-spread-function (PSF) was ~ 4 arcsecs at $12 \mu\text{m}$. The overall field of view was 104×104 arcsecs², which easily encompassed the whole galaxy which is over 40 arcsecs across.

The data were analyzed with the CAM Interactive Analysis software (CIA)². A dark model taking into account the observing time parameters was subtracted. Cosmic ray hits were removed by applying a wavelet transform method (Starck et al. 1997). Corrections of detector memory effects were done applying the Fouks-Schubert’s method (Coulais & Abergel 2000). The sky was subtracted using the emission from areas of the map well outside the galaxy and its value was within the one expected from the coarse DIRBE zodiacal maps. The flat field correction was performed using the library of calibration data. Finally, individual exposures were combined using shift techniques in order to correct the effect of jittering due to the satellite motions (amplitude ~ 1 arcsec). Based on our experience with ISOCAM data reduction and application of the above methods to a large set of observations, we estimate that the absolute uncertainty in our photometry measurements is less than 20%.

2.2. Ground-based Radio and Millimeter Observations

² CIA is a joint development by the ESA astrophysics division and the ISOCAM consortium

Observations were made with the D-array of the VLA on August 25 1992 at 4.9 ($\lambda 6$) and 8.4 GHz ($\lambda 3.5$ cm). These data were flux and phase calibrated, bad data were flagged and ignored, and final maps were made using the AIPS routine IMAGR. The effects of sidelobes were removed using the CLEAN algorithm, resulting in images of NGC 985 with synthesized beam sizes of 19.25×13.23 arcsecs ($\lambda 6$ cm) and 10.67×7.55 arcsecs ($\lambda 3.5$ cm).

The $^{12}\text{CO}(1-0)$ observations of NGC 985 were carried out with the Berkeley-Illinois-Maryland Association (BIMA) 10-element millimeter array (Welch et al. 1996) at Hat Creek, northern California. The preliminary BIMA observations were carried with one full track (7–8 hrs) of C array and D array observations in April 18 1998 and June 22 1998, respectively. A nearby phase calibration source 0238+166 was observed for several minutes before and after every half-hour of observations of NGC 985. Further observations with both the C array in May 21–24 1999 (three 6hr tracks and one short 3hr track), and the D array in July 15 and 17 1999 (two 3–4hrs tracks). The source 0339-017 was observed as a phase reference instead of 0238+166 during this observing because it was closer to NGC 985, and was bright enough to be used at this time (the source is variable). Individual antenna system-temperatures averaged 350 K, and were typically within the range 250 to 550 K. Mars and/or Uranus was observed for flux calibration. These data were flux and phase calibrated, and bad data flagged and channel maps made using the MIRIAD software. The synthesized beam of the final maps was 11.94×6.81 arcsecs with a position angle of -1 degrees. The receivers were tuned to 110.50 GHz corresponding to a redshift of $z = 0.043$, and the correlator was configured to cover a total velocity range of just over 1500 km s^{-1} at a spectral resolution of $\sim 8 \text{ km s}^{-1}$ (3.1 MHz).

A data-cube containing 40 channel maps was made, each channel covering a velocity width and separation of 25 km s^{-1} , centered on the heliocentric velocity of $12,934 \text{ km s}^{-1}$, and so cover a velocity range of almost 1000 km s^{-1} . Those maps with bright emission were CLEANed to remove the effects of sidelobes. Subsequent analysis of these data was performed in AIPS and MIRIAD.

2.3. Astrometry

As the next section shows, a large offset is found between the peak in the map of CO column densities, and the position of the AGN as defined by observations at radio and IR wavelengths. Because our observations were made under excellent conditions over seven different tracks with two arrays, BIMA was expected to return exceptionally high-precision astrometry. However to confirm this, we constructed maps of the galaxy by splitting the observations into two separate independent data-sets which used different combinations of phase calibrators and array configurations. The results showed identical emission features with excellent positional and flux agreement. We are therefore confident that the BIMA astrometry is of very high quality.

Similar arguments can be made for the VLA data which

has subarcsec accuracy, and the AGN core was independently observed by Ulvestad & Wilson (1984). Later in the paper we also compare our observations with UKIRT K-band IR images published previously by Appleton & Marcum (1993). These deep observations were registered to the astrometrically accurate 2MASS K-band image of NGC 985³ while the details of the registration of the MIR images is discussed in the next section. We are therefore confident that the registration of all the various datasets used in the forthcoming discussion are accurate to an arc-second or better – an angular scale much smaller than the observed offset in the CO distribution – the result that prompted us to perform these checks.

3. IMAGING RESULTS AT DIFFERENT WAVELENGTHS

3.1. Visible, IR and Radio Continuum Comparisons

The images obtained with ISOCAM at wavelengths of 4.5, 9.62, 11.4 and $15 \mu\text{m}$ respectively are displayed in Figure 1a-d. For reference, Figure 2a shows a contour map of the $15 \mu\text{m}$ emission superimposed on a grey-scale R-band image of the galaxy. We also present in Figure 2b the MIR spectral energy distribution (SED) of the nucleus, the properties of which are discussed in detail in Section 7. The $15 \mu\text{m}$ filter is the broadest and has the best signal to noise ratio of the four filters used. The images obtained in the three of the longer wavelength filters (Fig. 1b, c, and d) show very similar MIR distributions. The strongest emission comes from the nucleus of the galaxy and considerable extended emission is present. Emission is also seen near the two optically prominent H II regions in the western part of the outer ring. In addition fainter emission is detected immediately adjacent to the nucleus to the west, especially in Figure 1c and d along the optically prominent emission ridge. Only the center of the galaxy is detected at $4.5 \mu\text{m}$, but observations made with this filter are less sensitive than those made at other wavelengths.

Table 1 lists the MIR fluxes of the four ISOCAM filters for the central bulge/nucleus and for the bright “knot” seen near the western H II regions in the ring. Additional MIR observations of NGC 985 from the ground had also been performed by Maiolino et al. (1995) who found that the $10.6 \mu\text{m}$ (N-band) flux density within a 5.3 arcsec aperture centered on the nucleus of NGC 985 is 143 mJy. This agrees to better than 10% with the average flux density we obtained at with the 9.7 and $11.4 \mu\text{m}$ ISOCAM filters, and is conclusive proof that the majority of the $10 \mu\text{m}$ flux from NGC 985 is very centrally concentrated, since the ISO flux was determined over a much larger aperture than the ground-based observation and yet the same flux was observed. This is very different from the situation at $2.2 \mu\text{m}$, where the AGN’s contribution is much smaller than that of the stellar bulge (see Section 4) in the inner regions.

In order to register the MIR maps with the optical, near-IR, and radio maps, we could not assume that the absolute astrometry of ISO was better than a few arcsecs (unlike the relative astrometry which is much more accurate). We have made the reasonable assumption that the bright peak in the $15 \mu\text{m}$ map corresponds to the Seyfert nucleus detected at radio wavelengths. We registered this peak to the

³ We also independently checked the astrometry in the 2MASS image by comparing the position of a foreground star in the northern portion of the image with an astrometric measurement made in the optical by (Jeske 1986). They showed perfect agreement.

corresponding peak found from the VLA radio maps. Figures 3a and b show the radio continuum maps corresponding to a wavelength of 6 and 3.5 cm respectively. Figure 3c shows the 3.5 cm map superimposed on the R-band image of the galaxy. The 3.5 cm map, which has the better spatial resolution, shows a bright radio source we associated with the Seyfert nucleus, and a second component which lies to the west just inside the outer ring. The radio fluxes are given in Table 1. We fitted a Gaussian to the peaks in both radio maps (using the AIPS routine IMFIT) to determine an accurate position for the nucleus. Both positions agreed within a fraction of an arcsec. The centroid in both maps was found to occur at $\alpha(\text{J2000}) = 02^{\text{h}}34^{\text{m}}37.74^{\text{s}} (\pm 0.01^{\text{s}})$ and $\delta(\text{J2000}) = -08^{\circ}47'15.0'' (\pm 0.27'')$.

One potential difficulty of using the position of the radio core for the ISO image registration is the possibility that the nucleus might be heavily obscured, even at MIR wavelengths, (e.g. Rigopoulou et al. 1999; Soifer et al. 1999, 2001), and the peak may not be spatially coincident with the radio nucleus. However we can exclude this possibility because we find excellent positional agreement between the radio nucleus (above) and a K-band image of the nucleus obtained from the astrometrically accurate 2MASS survey (Skrutskie et al. 1997). Since the position of the near-IR nucleus and the radio nucleus correspond, we can safely assume that obscuration is not a factor in determining the position of the AGN core at wavelengths longward of $2 \mu\text{m}$.

Figure 4 displays the 3.5 cm radio map superimposed on images made at $15 \mu\text{m}$ with ISOCAM (Fig. 4a), and at $2.2 \mu\text{m}$ with UKIRT (Fig. 4b, an image based on near-IR data from Appleton & Marcum 1993). This shows that the MIR and radio emission have similar distributions. Figure 4b shows that the radio source is associated with the eastern (brighter) component of the double nucleus. No obvious radio emission is found associated with the second nucleus, consistent with the suggestion by Pérez García & Rodríguez Espinosa (1996) that the second nucleus is not active⁴.

3.2. CO Distribution and Integrated Properties of NGC 985

Figure 5 shows a map of the integrated $^{12}\text{CO}(1-0)$ emission from NGC 985 superimposed on optical (Fig. 5a), $15 \mu\text{m}$ MIR (Fig. 5b), and 3.5 cm radio maps (Fig. 5c) of the galaxy. The emission is distributed in an elongated structure with two almost equal peaks separated by 13–15 arcsecs. A weaker third CO concentration is seen to the west, near a part of the ring which contains two powerful H II regions. No emission is seen associated with the large stellar ring which loops to the north of the nucleus/budge at large radii.

A striking offset of about 5 arcsecs is found between the main body of CO emission, and the bright radio/IR peak. Indeed the majority of the CO avoids the nucleus and is mainly concentrated to the west, where some of it is associated with the peculiar ridge of optical/IR emission extending away from the center. Such offsets are unusual in collisional galaxies, where either the gas is cen-

tered on (or straddles) the nucleus. In the unusual case of Arp 220, a galaxy with two nuclei probably undergoing a major merger, the CO is mainly concentrated between the two nuclei in a massive molecular disk (Scoville et al. 1997), but is still centrally concentrated.

Very few ring galaxies have been observed in CO with high resolution. In a few cases, single dish observations have provided some indication of molecular distribution on the scale of the large outer rings. The major single-dish study of ring galaxies by Horellou et al. (1995) shows that some systems (e.g. II Hz 4) have emission concentrated in the outer star-forming rings (see also Higdon et al. 2000, for AM0644-741). However, only two systems, Arp 118 and Arp 143, have been published with high spatial resolution (Gao et al 1997; Higdon et al. 1997). In Arp 118 most of the CO is found in a powerful star forming ring, with little CO(1-0) emission from the center of the galaxy. In contrast to this, Arp 143 (Higdon et al. 1997) and the Cartwheel (Horellou et al. 1998) have CO concentrated towards the center.

We have constructed an integrated spectrum of the CO emission from the galaxy which is shown in Figure 6, along with arrows indicating the velocities of the two nuclei. Also shown is the range of velocities quoted in the single-dish study of NGC 985 by Horellou et al. (1995). This underestimates the full range observed, since it shows the range at FWHM for some representative spectra (an integrated spectrum is not provided in that work). Their IRAM 30-m $^{12}\text{CO}(1-0)$ observations, obtained with a 22 arcsec beam and performed over several pointings across the galaxy, agree closely in terms of overall velocity spread and line-shape with the BIMA spectrum. There is also excellent agreement between the BIMA fluxes and the IRAM observations.

Table 2 presents a compilation of the observed and derived molecular gas properties based on these observations, along with published single dish CO and upper limits to the H I mass in the system from other work. As the table shows, the BIMA observations retrieve 100% of the single dish flux. Adopting the “standard” conversion from CO flux to H_2 mass (see Young & Scoville (1991)) given by $M(\text{H}_2) = 1.18 \times 10^4 F_{\text{CO}} D^2 (1+z)^{-1}$, with $D = 170 \text{ Mpc}$, then $M(\text{H}_2)$ is found to be $1.8 \times 10^{10} M_{\odot}$. This conversion factor is highly uncertain, but we adopt a standard conversion for comparison with other work. The ratio of $L_{\text{IR}}/M(\text{H}_2)$ for NGC 985 is 10 (see Table 2). This indicates that the present star formation activity in NGC 985 is comparable with a local starburst galaxy, but not as high as typical ULIRGs or quasars (Sanders & Mirabel 1996; Evans et al. 2001). From a star formation point of view, NGC 985 has the potential to become significantly more luminous and more star formation efficient in the future.

We note that no neutral hydrogen has yet been detected from NGC 985. An upper limit to the H I mass of $< 3.6 \times 10^9 M_{\odot}$ is derived from Heckman et al. (1978) after correcting their upper limit for our adopted value of the Hubble constant, and assuming that the H I velocity-

⁴ P. N. Appleton, in a personal communication, mistakenly reported to J.M. Rodríguez Espinosa that the second nucleus was also a radio source, a report that was included in their paper on the double nucleus (Pérez García & Rodríguez Espinosa 1996). Although it is true that the radio source appears double, the second component is seen on a much larger scale and is not associated with the second nucleus (Figure 3c). The mistake is regrettable.

width is similar to that of the CO profile. This leads to a $M(\text{H}_2)/M(\text{H I})$ ratio of greater than 5.5 implying that *the bulk of the cool interstellar medium (ISM) in NGC 985 is in molecular form*⁵. Mirabel & Sanders (1989) have shown that $M(\text{H}_2)/(M\text{H I})$ ratios as large as 4-20 are usually found in advanced merger galaxies that have the highest far-infrared to optical flux ratios, are ultraluminous in the infrared, and exhibit OH megamaser emission. In this context, if the upper limit for the HI mass is confirmed, NGC 985 could be considered as an ultraluminous infrared galaxy in the making. We will discuss this and another possibility later in the paper.

4. CO KINEMATICS – EVIDENCE FOR TWO DYNAMICALLY DISTINCT POPULATIONS

One reason that the main concentration of CO emission is not centered on the nucleus of NGC 985 may have to do with the peculiar motions present in the CO gas. To demonstrate this, we have constructed a data cube which represents the observed CO column densities in each of 40 channels covering a velocity spread of almost 1000 km s^{-1} centered on the velocity of the system.

Figure 7 shows a series of channel maps over the range of velocities $12,639 \text{ km s}^{-1}$ to $13,089 \text{ km s}^{-1}$ in steps of 25 km s^{-1} intervals—the range in which significant CO emission is detected. We note that only a subset of the full range of velocity coverage is shown here, since the rest of the channels show little significant emission above an rms noise of 11 mJy beam^{-1} . The first contour is close to the 3σ level (30 mJy beam^{-1}).

To aid the discussion, we also constructed a composite of the various emission features from Figure 7 and superimposed onto the K-band UKIRT contours of the galaxy. Because the kinematics of the galaxy is unusually complex, we have split the composites into three parts, representing the low, medium, and high velocity regimes in the data cube (Fig. 8a, b & c respectively). In the following paragraphs we will demonstrate that in Fig. 8a, b, the concentrations of CO are somewhat randomly distributed about the nucleus showing very little obvious coherence from one channel to the next, whereas, Fig. 8c shows emission that is much more easily comprehended, as it displays very clear channel-to-channel coherence. This is not a signal-to-noise effect, since all the features in the maps are significantly above the noise, and are identifiable as emission in the single-dish observations. Later, we will demonstrate that the emission features seen in the first two panels of Fig. 8 may have distinctly different dynamical properties from the more coherent high-velocity emission.

The lowest velocity channel maps in which CO is detected are shown in Figure 8a, covering the range $12,764$ to $12,889 \text{ km s}^{-1}$. At these velocities, gas is seen covering the eastern AGN (N1), but shifts away, first to the south ($V = 12,789 \text{ km s}^{-1}$), and then to the west at velocities higher than $12,814 \text{ km s}^{-1}$. Indeed at velocities close to the systemic velocity of N1 ($12,814 \text{ km s}^{-1}$ see Arribas et al. 1999) the CO emission is offset from N1 by a few arcsecs and does not cover either N1 or the western nucleus N2. The tendency of the brighter emission to be offset to

the west of the AGN is the reason why the peak in the integrated map in Figure 5 is offset from N1.

In Figure 8b we show the gas at intermediate velocities. Here again, as in Fig. 8a, emission is seen which has little obvious spatial coherence from one channel to the next. In some channels, the gas is roughly associated with the ridge of starlight seen by Rodríguez Espinosa & Stanga (1990) extending from the nucleus to the west. We note that in one channel ($V = 12,939 \text{ km s}^{-1}$) there is a component of the CO seen to the northwest of the AGN. This corresponds to the position of the possible MIR arc discussed later in Section 6, although this could be coincidental. However, for the most part, the intermediate velocity gas is only loosely associated with the linear optical ridge which dominates the western side of NGC 985.

The high velocity emission from NGC 985 begins to show more noticeable channel-to-channel coherence. This is one of the features that distinguishes it from the lower-velocity emission. At $V = 12,989 \text{ km s}^{-1}$, gas is seen over a wide range of positions, extending all the way from the western extreme edge of the ring to the nucleus N1 (this also shows that the CO emission spectrum in the direction of the nucleus contains multiple components). Emission over successively higher velocities is seen to shift progressively towards the outer ring, bending northwards (at $V = 13,039 \text{ km s}^{-1}$) into the region of two powerful H II regions. In these channels, a fainter “finger” of emission extends back towards the double-nucleus. At extremely high velocities the emission is concentrated at the end of the stellar ridge. The highest velocity gas, and that with the highest velocity dispersion (150 km s^{-1}) is seen approximately 14 arcsecs west of the nucleus at the position $\alpha(\text{J2000}) = 02^{\text{h}}34^{\text{m}}36.9^{\text{s}}$, $\delta(\text{J2000}) = -08^{\circ}47'18''$. This position corresponds to a region in the linear optical emission ridge which exhibits the strongest H α emission as discussed by Rodríguez Espinosa & Stanga (1990) and Appleton & Marcum (1993).

The molecular gas distribution and kinematics at first seem quite complicated and difficult to understand. However, some insight into the behavior of the clouds comes when we realize that there may be two different kinds of dynamics being exhibited here: a) cloud-complexes that are distributed at random positions close to the nucleus and have no obvious optical/IR counterpart, and b) cloud structures that have well-defined spatial-velocity coherence. These latter clouds tend to be associated with the obvious optical/IR features, and look similar to the structures we are familiar with in studying gas in galaxies (i.e. spiral arms, rings, tidal loops etc).

Many of the individual “clouds” we refer to here are quite massive, a few $\times 10^8 M_{\odot}$, and we will refer to them as Super Giant Molecular Clouds (SGMCs). To show that two dynamically different CO emission features may be present, we show in Figure 9 two ways of visualizing them. Figure 9a shows the distribution of position angles of the SGMCs (north through east) relative to the AGN (nucleus N1) as a function of the radial distance from N1. These are the coordinates of the centroids of each SGMC measured channel-by-channel from the channel maps. The

⁵ Contrary to NGC 985, the Seyfert galaxy NGC 1144 (= Arp 118) Bransford et al. (1999) showed the HI and CO distribution and kinematics in that galaxy were highly peculiar as a result of a violent interaction. Even in that case, the observed $M(\text{H}_2)/M(\text{H I})$ ratio was 2.6 – a factor of at least two lower than in this case.

centroid of each SGMC was determined (to within 1–2 arcsecs = 0.8–1.6 kpc) if it was represented by two or more contour levels ($>4.5\sigma$) in the channel maps of Fig. 7. In some cases where extended emission is observed, only the brighter obvious clumps were extracted. However, in most cases the identification of a SGMC feature was straightforward and unambiguous. From Figure 9 it is obvious that within a radial distance of 9 kpc (10.9 arcsecs) of the center, the SGMC complexes are distributed in a random manner with respect to the nucleus, whereas, the average nature of the emission changes and becomes more ordered and coherent at larger radii. This transition was noted in the discussion of the previous figure, but is put on a more quantifiable footing here.

The separation of the SGMCs into the two components is not restricted to their different spatial distributions, but also is apparent in their different kinematic behavior. In Fig. 9b, we plot the velocity of the SGMCs (relative to the AGN systemic velocity of $12,814 \text{ km s}^{-1}$) as a function of radial distance from the nucleus. It can be seen that within 9 kpc (representing the area of the “randomly distributed” SGMCs) the velocities of the clouds are distributed equally on either side of the systemic velocity of the active nucleus N1, and the clouds appear to dynamically related to the nucleus. However, for the emission at larger radii (mainly those associated with the optical/IR ridge feature) the clouds cluster together in one region of the diagram, a result of spatial and kinematic coherence.

The implication of Fig. 9 is that the CO emission in NGC 985 exhibits two distinct kinds of dynamics. A randomly distributed (radius $< 9\text{--}10$ kpc) SGMC system, centered both spatially and in velocity-space on the nucleus N1, and a more distant coherent SGMC system which is highly correlated with obvious optical/IR galaxy components.

4.1. Is the “random component” rotating?

It is common when analyzing data cubes containing spectral line data to create “moment” maps (isovelocity and velocity dispersion) which are often useful in helping the astronomer interpret their data. Although we constructed such maps early in our analysis of these data, we felt the maps were misleading because, i) the data cube contains many places where multiple velocity components are seen along the line of sight and, ii) the cube contains isolated cloud components which are not obviously related to another. This stochasticity in the velocity field leads to a very confused pattern in the isovelocity map, making it difficult to interpret. Despite these reservations, *some limited* inference can be drawn if we divide it up into two velocity regimes.

In Fig.10a and b we show the isovelocity maps for the cube covering the velocity range $12,684$ to $12,934 \text{ km s}^{-1}$, and $12,984$ to $13,034 \text{ km s}^{-1}$ respectively. This separation roughly corresponds to the CO emission associated with the randomly distributed nuclear-centered clouds (Fig.10a), and higher-velocity more coherent clouds (Fig.10b) discussed earlier⁶. Despite some major excursions from regularity, Fig.10a shows that the isovelocity contours for the nuclear-centered low-velocity system may

show the signature of rotation or gas streaming motions, even though they are observed as discrete clouds with somewhat random *positions* relative to the nucleus. The higher velocity emission is associated with mainly identifiable optical/IR features in the outer galaxy and can be seen in Fig.10b. Its pattern confirms our earlier observation that the gas in the higher velocity channels behaves differently from the low-velocity emission – the steepest velocity gradient being associated with the outer eastern ring.

5. THE DYNAMICS OF THE LOW-VELOCITY CO CLOUDS AND THE IONIZED INNER DISK OF NGC 985

In the previous section we presented evidence that the CO emission seen within 10 kpc of the double nucleus of NGC 985 is composed of bright clumps of emission randomly distributed about the center, but showing a general east to west drift (as is demonstrated in Fig.10a) which might be interpreted as rotation, or at least coherent streaming motions. What is the dynamical state of this cloud system and is it coupled to the motions of the ionized gas and stars seen rotating in quite orderly motions near the nucleus of NGC 985?

Arribas et al. (1999) showed that *both the stellar and emission line velocity field* in the central few arcsecs around the nucleus of NGC 985 is consistent with an orderly rotating disk, with a kinematic axis along a PA of -45 degrees (this is the same positional angle that connects the two nuclei). It is already clear from the isovelocity map of Fig.10a that the east-west drift seen in the CO velocity field *does not* share the same kinematic major axis as the ionized gas. Indeed, if we ignore the obvious irregularities in the CO velocity field, and naively interpret Fig.10a as indicative of a rotating disk, it would have a kinematic major axis of approximately -90 degrees—quite different from the kinematic major axis of the more-uniform ionized disk.

We can explore the possible connections between the CO emission and the ionized disk more clearly in Fig.11, which shows the position of the CO emission centroids of eleven of the centrally concentrated SGMCs (and their velocities) superimposed on the isovelocity “spider” diagram of the *ionized* gas from the work of Arribas et al. (1999). This figure shows the east-west drift in the SGMC positions with increasing velocity, but confirms that the clouds are definitely *not* co-rotating with the ionized gas disk. For example, if the CO clouds were simply clumps of molecular material moving in circular orbits with the ionized gas, then each CO centroid should lie on a corresponding isovelocity line as defined by the velocity field of the ionized gas. In contrast to this, most of the CO centroids lie at velocities which are discrepant from the velocity of the ionized gas at the same position. A number of the CO centroids lie outside the region where the ionized gas velocity field was measured, but even in those cases, the velocities corresponding to those CO centroids are inconsistent with any simple extension of the “spider” diagram of the ionized gas. The CO clouds are most discrepant to the east and south of the nucleus, where they have velocities which are approximately 100 km/s too low for the

⁶ We stress that even this simplistic division of the cube obscures some of the details that are best seen in Fig 8. For example, the isovelocity contour at $12,934 \text{ km s}^{-1}$ in Fig.10a does not smoothly join in a coherent way with the contours at $12,984 \text{ km s}^{-1}$ shown in Fig.10b – a result of multiple components of emission along several lines of sight.

corresponding ionized gas velocity. Only one SGMC (at $V = 12989$ km/s) has the same velocity as the ionized gas at that same position (it may be coincidental-but this is close to the position of the second (non-active) nucleus). The CO emission, while exhibiting the same general trend of east-west motion, appears only loosely coupled to the ionized disk, and shows some highly discrepant velocities, especially to the south and east.

5.1. An Unstable Collapsing Disk or Clouds Dominated by Random Motions?

In this section we will explore two different dynamical states for the inner CO cloud distribution. The first will assume that the east-west drift seen in the CO centroids is due to rotation, and we will show that these rotational velocities are insufficient to stop the CO from sinking towards the center when compared with the likely mass in old stars present in NGC 985. A second alternative also exists, that the clouds travel on non-circular orbits throughout the center-allowing for the possibility that they are marginally stable. The latter, if true, implies that the central CO distribution is highly disturbed, perhaps a result of interactions between the CO clouds and an AGN wind—an extra complication that must be taken into account when modeling the evolution of gas in merging gas-rich systems.

If we were to interpret the overall east-west trend of velocity with position across the center of NGC 985 in the CO clouds as being rotation, we can ask what mass would be required to keep the clouds in stable circular motion. Taking the CO centroids both east and west of the nucleus to be representative of the maximum velocity spread (275 km s^{-1}), this implies that the mass needed keep the clouds in circular orbits at a radius of $r=10$ arcsecs (8.25 kpc) would be $2.89 \times 10^{10} (\text{cosec } i)^2 M_{\odot}$, where i is the inclination of the disk. Assuming an average inclination $i = 45$ degrees, this would imply a total mass within 8.25 kpc needed to produce circular orbits of $M_{\text{circ}} = 6 \times 10^{10} M_{\odot}$. We will show, in what follows, that this mass is unrealistically small, implying that if the clouds are in rotation, they have insufficient velocity to remain in circular orbits, and are likely to be falling inwards towards the center, a result that has implications for the future evolution of NGC 985.

Before we estimate the minimum gravitational mass in the inner region of NGC 985 using the flux in K-band light, we will make another estimate of the mass required for an equilibrium configuration for the CO clouds which does not make explicit assumptions about the shape of the orbits. Such an approach is justified if we believe (as concluded above) that the CO clouds may not be in circular orbits. The method, called the projected mass estimator, was devised by Bahcall & Tremaine (1981) for the problem of the mass of dark matter in small groups of galaxies. This may be more appropriate for a system in which we have only a small number of “test particles” (the SGMCs) moving in the potential of the galaxy. The method finds a weighted mass for a system assuming that the “test particles” probing the mass are gravitationally bound to the central mass. Making the least assumptions about the ellipticity of the orbits, the relevant equation is:

$$M_o = \frac{24}{\pi G N} \sum_{i=1}^N v_{zi}^2 R_i \quad (1)$$

where v_{zi} is the difference in the recessional velocity between the i^{th} SGMC, and the central massive object. R_i is its projected distance from the center, and N is the total number of SGMCs.

Putting in the values for the randomly distributed SGMCs in the above equation, and assuming the velocity and position of the AGN are the barycentric coordinates, the total projected mass is found to be $M_o = 1.43 \times 10^{11} M_{\odot}$. This is more than twice the mass found assuming circular orbits, but uses all the cloud velocities rather than just those at the velocity extremes of the distribution, as in the circular velocity case.

How do these dynamically estimated masses compare with the mass in stars in the inner regions of NGC 985? We can determine a lower limit to the mass of stars by estimating the mass associated by old stars via the relationship developed by Thronson & Greenhouse (1984). This approach uses the K-band luminosity of a galactic region (they applied it to the center of M51) calibrated via measurements of the mass in old stars in the solar vicinity. Normally such a calculation could not be applied to a galaxy dominated by a powerful AGN, but Appleton & Marcum (1993) showed that at $2.2 \mu\text{m}$, the bright nuclear source is only a minor component of the K-band light—which is dominated by old stars in the bulge. We are therefore able to remove the contribution of the AGN from our calculation. We emphasize that this is likely to be an underestimate of the true mass, since it neglects younger stars and the possible contribution of dark matter.

Using the maps and photometry of Appleton & Marcum (1993), we are able to conclude that within a diameter of 22 arcsecs (18 kpc) the total K-band flux is 33 mJy, of which only 13 mJy (39%) originates within 2×2 arcsecs of the AGN. Hence the total K-band flux from the region of the random SGMC component is approximately 20 mJy. This corresponds to a total mass in old stars of $M_{\text{oldstars}} = 1.5 \times 10^{11} M_{\odot}$. We consider this a conservative lower limit to the true mass.

This lower limit to the stellar mass in the inner regions of NGC 985 is larger than the mass estimated from the velocity and positions of the CO clouds assuming reasonable circular orbits, $M_{\text{oldstars}}/M_{\text{circ}} > 2.5$, and is closer (but still larger than) the mass found assuming the clouds travel on non-circular orbits. This implies that either the gas is spiraling into the center on a relatively rapid time-scale, or that the gas clouds are exhibiting high peculiar motions—perhaps some infalling and some expanding outwards from the center. In both cases, this argument, when combined with the obvious discrepancies with the velocities of the regularly rotating *ionized* gas disk suggests that the CO clouds are in a highly disturbed state and are probably not in equilibrium with the gravitational potential.

6. NUCLEAR ASYMMETRIES - FURTHER EVIDENCE FROM ISO

The CO distribution and kinematics are not the only features of this galaxy which suggest that the inner galaxy is in a non-equilibrium state. In Figure 12a we show that

the MIR emission near the nucleus is not symmetrical, but that there is a bright arc or shell to the north and west of the nucleus at an angular distance of about 5 arcsecs (see also Appleton et al. 2000). The figure shows the application of a simple “unsharp mask” technique to the $\lambda 15\mu\text{m}$ ISOCAM image. This filtering technique is sensitive to small-scale structure in the image on the scale of a few arcsecs.

To further explore this feature, which is also obvious on independent images taken at other wavelengths (the $9.62\mu\text{m}$ and $11.4\mu\text{m}$ images), we performed a series of experiments using the theoretical monochromatic ISOCAM PSF for $\lambda 15\mu\text{m}$, smoothed appropriately to take into account the width of the filter. The PSF was also rotated to match exactly the micro-scan direction of the observations.

We show in Figure 12b the result of an iterative removal of the PSF from the peak of the Seyfert nucleus. The image shows the result of three iterations of removal, in which the PSF was subtracted from the peak in the map with a loop-gain of 0.5 (similar to the technique CLEAN of Högbom 1974, used in radio astronomy). The following conclusions were drawn from our experiments: a) The nuclear source itself is slightly extended on the scale of a few arcsecs and, b) there is an excess of emission to the north and west of the nucleus which cannot be explained by the properties of the detector or the observing technique. Furthermore, these bright regions fall on the null of the first Airy ring of the optical system – again an indication that the emission is real.

In conclusion, we believe that the ISO images show, on several independent filters, evidence of an asymmetry in the dust distribution near the nucleus which we are unable to explain as an instrumental artifact. The emission may be shell-like, but because the emission falls so close to the bright nucleus we would prefer to await higher resolution observations before making a definitive statements about its morphology. However, the emission does support the view that the dust and gas are highly disturbed and not always directly coupled, since this asymmetric dust feature is *not* seen in the same direction as the main CO distribution (although, as discussed in Section 4, there may be a faint CO counterpart seen in one channel).

7. MID-IR SPECTRAL ENERGY DISTRIBUTION

It has been shown (Lutz et al. 1998; Laurent et al. 2000) that a galaxy hosting a dominant AGN is clearly different in the MIR from one dominated by a nuclear starburst because the AGN heats the dusty torus surrounding it. Perhaps because of grain destruction in the powerful AGN radiation field, the well known emission bands at 6.2, 7.7, 8.6, 11.3 and $12.7\mu\text{m}$ (usually attributed to Polycyclic Aromatic Hydrocarbons) are extremely weak or completely missing from the MIR spectrum of powerful AGNs, and this can provide an additional diagnostic if the MIR extinction of the nucleus is not too great.

To examine the MIR characteristics of the nucleus of NGC 985, we display in Figure 2b the four MIR flux densities measured over an aperture 12 arcsecs in diameter centered on the radio continuum peak (from Table 1). This aperture covers the majority of ISO emission associated with inner regions of NGC 985. The width of the corresponding ISOCAM broad-band filters is also displayed

with the horizontal lines. For comparison, we also show the MIR spectra of two very different emission regions, an AGN dominated MIR spectrum from the nucleus of NGC 1068 (see Fig. 4 of Le Floc’h et al. 2001), and a typical star formation-dominated MIR spectrum from knot B of the Antennae galaxies (see Vigroux et al. 1996; Mirabel et al. 1998). Both spectra have been redshifted to the same rest wavelength as NGC 985 and their flux was normalized to the $11.4\mu\text{m}$ flux of NGC 985.

An inspection of the SED in Figure 2b suggests that the longer-wavelength spectrum of the nucleus of NGC 985 looks more like a nucleus dominated by star formation, than one where the dust is heated directly by an AGN, since the spectrum of NGC 985 does not rise as fast as that of NGC 1068, especially in the 10–15 μm range. Only at $\lambda 4.5\mu\text{m}$ is there a hint of a “warm bump” from the slightly elevated flux at that wavelength. However, since this could be due to contribution from old stars of the bulge and we lack more definitive diagnostics in the 5–10 μm range (Laurent et al. 2000; Le Floc’h et al. 2001), further observations would be necessary to confirm this possible result.

It is of interest to note that our first-order deconvolution of the nuclear emission from the AGN (see Section 6) suggested that the nuclear emission maybe slightly extended relative to the theoretical PSF for the telescope. If so, we tentatively associate this emission with the stellar and hot-ionized gas disk which is seen in the central few arcsecs of the galaxy by Arribas et al. (1999) from optical observations. This inner rotating “disk” must be composed of both stars and ionized gas since both are seen to co-rotate along a line joining the two embedded galactic nuclei. The MIR observations may be pinpointing the formation of a proto-disk at the core of what will eventually become a collisional remnant. Could this be direct evidence for the formation of disk cores in elliptical galaxies? Higher resolution MIR observations should allow us to determine whether the MIR emission does indeed coexist with the inner rotating ionized disk seen by Arribas et al. (1999).

8. NON-NUCLEAR STAR FORMATION SITES IN NGC 985

We had seen from the CO, radio, and MIR maps that NGC 985 contains a bright ridge of stars, gas and dust that extends from the double nucleus all the way out to the stellar ring to the west. Furthermore, in the paper by Rodríguez Espinosa & Stanga (1990) it was shown that the entire length of the optical/IR ridge is populated with powerful H II regions, the most powerful of which lie towards the end of the ridge, and in two additional H II regions in the ring. Although the ISO observations show MIR emission associated with the bright H α emitting regions, we note that the MIR emission does not always mimic the brightness variations from the optical line-emitting regions. For example, the two bright H II regions in the outer ring (knot A and B in Rodríguez Espinosa & Stanga 1990) are much stronger in the ISO observations than the end of the linear structure (knots G & H of Rodríguez Espinosa & Stanga 1990), despite the fact that both sets of regions have very similar observed H α luminosities. Such differences may relate to differences in the relative populations of small and large dust grains in the various regions (as suggested by Wilson et al. 2000,

to explain differences in the MIR properties of the supergiant CO complexes found associated with star forming regions in the Antennae galaxies), or they could simply reflect different internal optical extinction within the optical nebulae.

One explanation for the high star formation rates seen along the linear ridge is suggested by the high velocity dispersion in the CO gas in this region (see discussion in Section 10). For example, Stanford et al. (1990); Wilson et al. (2000); Gao et al. (1997) have shown that in NGC 4038/4039, one of the most powerful star formation sites corresponds to a region of high CO velocity dispersion (the region called SGMC 4–5 by Wilson et al. 2000). In our case, we observe a similar phenomenon. In particular, the region towards the end of the linear structure corresponds to the highest velocity dispersion seen in the molecular gas (150 km s^{-1}). This region also contains some of the brightest star formation sites seen along the optical emission ridge, since knots G and H from Rodríguez Espinosa & Stanga (1990) have combined luminosities in the $\text{H}\alpha$ line of $7.1 \times 10^{40} \text{ erg s}^{-1}$, a value approximately 15 times the luminosity of the 30 Doradus nebula in the LMC.

Even the outer ring of NGC 985 has some odd characteristics. For example, we note from the overlays in Figure 2a, that although the MIR emission at $\lambda 15 \mu\text{m}$ falls almost on top of the contours of bright ring H II regions A and B of Rodríguez Espinosa & Stanga (1990), the CO emission (see Figure 5) falls significantly *inside* the ring, suggesting that the CO near the H II regions themselves has been destroyed, but the dust grains associated with the H II regions, clearly seen in the ISO maps, have not! This underlines the complex relationship between CO emission and dust emissivity in colliding galaxies – a point already made cogently by Wilson et al. (2000) for the NGC 4038/39 system.

To further complicate the star-formation story for NGC 985, we note that the radio continuum emission from the ring also fails to correlate spatially with either the optical, radio or the CO emission! The main $\lambda 3.5 \text{ cm}$ emission regions, seen in Figure 3, lies inside the bend in the ring, and the offset is significant. This offset between the radio continuum and the current star formation sites has been seen before in ring galaxies (e.g. Appleton et al. 1999) and may be the natural result of the propagation of a star formation wave through the outer disk of the target galaxy. The radio continuum emission, if created by cosmic rays from supernova explosions, will tend to lag behind the regions of current star formation site because time must elapse for the massive stars to explode.

We can attempt to estimate the number of supernova needed to create the observed radio continuum emission. Assuming that the the radio emission is predominantly non-thermal (the spectral index is -0.6 which suggests mix of thermal and non-thermal emission) then we can estimate the supernova rate from equation 8 of Condon & Yin (1990) :

$$L_{\text{NT}}(\text{W Hz}^{-1}) = 1.3 \times 10^{23} \left(\frac{\nu}{1 \text{ GHz}} \right)^{-\alpha} \left(\frac{R_{\text{SN}}}{1 \text{ yr}} \right) \quad (2)$$

where L_{NT} is the non-thermal radio luminosity, α is the radio spectral index, and R_{SN} is the rate of type II supernova. For the western radio component, the radio lumi-

nosity at 6 cm, $L(6\text{cm}) = 3.3 \times 10^{21} \text{ W Hz}^{-1}$, which corresponds to a maximum (assuming all non-thermal emission) SN rate $R_{\text{SN}} = 0.067 \text{ yr}^{-1}$. Is such a supernova rate reasonable, given the know rate of star formation in the giant H II regions near the radio component?

To test this, we can calculate the rate of type II supernova that would be expected from knots A and B combined (the adjacent knots to the radio emission region), based on the star formation rates in those H II regions. If we assume a Salpeter IMF and a reasonable cutoff to the upper mass limit on the IMF we reverse equation 12 of Condon & Yin (1990) to:

$$R_{\text{SN}} = L_{\text{H}\alpha}(\text{W}) / (1.1 \times 10^{36}) \text{ yr}^{-1} \quad (3)$$

Using the combined values for knots A and B from Rodríguez Espinosa & Stanga (1990) of $L(\text{H}\alpha) = 9.0 \times 10^{33} \text{ W}$, we find $R_{\text{SN}} = 0.01$, a factor of six times too low to explain the observed radio emission. However, when correcting for an internal extinction of 2 magnitudes based on optical spectra of the knots (Bransford et al. 1998) these rates come into reasonable agreement. We conclude that a burst of star formation in the past, with a magnitude similar to that currently occurring further out in the ring is quite capable of supplying the required cosmic rays needed to power the radio source.

9. UV ABSORBERS ASSOCIATED WITH CO EMITTING CLOUDS: COINCIDENCE OR PHYSICAL CONNECTION?

Several strong absorption features are seen in the blue wings of the broad $\text{Ly}\alpha$ and N V 1238/1242 (S. Penton & J. Stocke private communication). Intrinsic lines of this kind are found in roughly 15% of Seyfert galaxies, and seem to represent a population of warm clouds expelled in a nuclear wind. Independent evidence for warm absorbers in NGC 985 are found from the X-ray analysis of Brandt et al. (1994). The HST spectrum kindly shared with us by S. Penton and J. Stocke show six absorption lines seen in $\text{Ly}\alpha$. All except the most blueshifted line is also seen in absorption against N V. The velocities for the lines are listed in Table 3. The highest velocity line, around $13,065 \text{ km s}^{-1}$ in $\text{Ly}\alpha$, is narrow and isolated (FWHM of approximately 50 km s^{-1}) whereas the other lines, although also narrow, may be part of a broad blended system extending over a full width of 600 km s^{-1} . Nevertheless, these individual narrow features are (except the most blueshifted one) seen in absorption against N V $\lambda 1239, 1243$ as well.

Interestingly, we find that the two most red-shifted lines correspond to velocities at which CO gas is seen projected against the nucleus. In fact, from Fig. 8 it can be seen that, because of the off-set in the main CO distribution, gas is seen against the nucleus in only three regimes – between $V = 12664\text{--}12689$, $V = 12764\text{--}12789$ and $V = 12989\text{--}13039 \text{ km s}^{-1}$. The highest and lowest velocity CO emission feature seen against the nucleus correspond quite well to the velocities of the warm absorbers.

The high velocity absorption line (and the CO in emission) lies close to the systemic velocity of the non-active nucleus N2. The narrow width of the UV absorber implies that it might be ISM material associated with N2 (despite this being seen in absorption against N1).

The UV absorber system observed at $V = 12,670 \text{ km s}^{-1}$ also seems to correspond to the velocity of gas seen in

CO emission in front of the nucleus – in fact it corresponds to CO seen in two adjacent channels (spread over 50km^{-1}). These emission features form part of the randomly-distributed cloud population discussed earlier. Could the UV absorber and the CO emission be related – perhaps through an interaction of the AGN wind with the infalling clouds? One argument against this is that the CO clouds are cold, and yet the UV absorption-line clouds are warm. However, if an infalling cloud was, through the chaotic nature of the infall, to encounter an AGN-driven wind, it may become heated and its outer envelope may well become ionized. Although our CO observations cover two more of the uv-absorption line velocities, no emission was detected from the more blue-shifted components. Perhaps dense molecular clouds encountering the wind do not survive long, and are evaporated rapidly as they become entrained in the wind. We note that this may be the first time there had been a possible identification between intrinsic Ly α absorption line components and CO emission, although CO absorption lines have been discovered associated with intervening galaxies in the direction of millimeter bright high-z sources (e.g. Wiklind & Combes 1994).

10. NGC 985: PRESENT AND FUTURE PROSPECTS

The presence of a faint extended ($r = 10\text{kpc}$) and probably unstable population of SGMCS in the inner regions of NGC 985 is generally unusual for merging or collisional systems, although it does share some similarities with some well studied cases. For example, in the case of Arp 220 (Scoville et al. 1997), the CO, although highly concentrated towards the center, involves two embedded nuclei revolving within a (CO rich) rotating disk. Similarly, the peculiar ring galaxy Arp 143 (Higdon et al. 1997), like NGC 985, also contains two molecular components, one concentrated in the ring, and another concentrated in the nucleus. Both these systems have highly centralized CO distributions in rapid rotation and may suggest one possible direction in which NGC 985 is evolving. Alternatively, as we shall discuss below, NGC 985 may actually have already been through the dense centrally-concentrated stage (ULIRG stage–Sanders & Mirabel (1996)), and its diffuse clumpy CO distribution may represent the early stages of the disruption of the central disk by a combination of AGN and star-formation-driven winds from the center. Both possibilities could explain the present state of NGC 985.

10.1. *NGC 985: The Formation or Destruction of a ULIRG?*

Despite an incomplete knowledge of the details of the interaction, the observations presented here provide a compelling case for a bright future for NGC 985! The peculiar CO distribution, decoupled as it is from the inner rapidly rotating ionized and stellar disk, suggests the gas is highly disturbed, and some of it may be either falling towards the center (see Section 4), or may be in marginally stable, but non-circular orbits. There are however many questions that are raised by the observations. What will be the fate of the $2 \times 10^{10} M_{\odot}$ of molecular gas over time? What is the significance of the intrinsic warm absorbers seen in the UV and X-ray spectra of the Seyfert nucleus and their relationship to the random component of the CO clouds? Finally, is NGC 985 likely to become much more IR-luminous in

the future, evolving towards a ULIRG state, or is there evidence that it has already passed through that state and that its activity may well be in decline?

The current observations provide only partial answers to these questions. Firstly, in the absence of a disturbing nuclear wind, the CO reservoir cannot remain out of equilibrium for more than a few crossing times, given the dissipative nature of gas. Taking the overall scale of the CO structure (about 20–25 arcsecs = 16–20kpc) and dividing by the total velocity-spread in the CO (Fig. 6) of 400km s^{-1} , provides a rough timescale for the dissipative collapse of the gas of 45–50 Myrs. If the gas is indeed infalling and we conservatively assume that 2 such periods would be needed to allow the gas to settle, then we might expect the large-scale accretion of the gas into the center to occur over the next 100 Myrs. If this was a smooth process, this would provide an average accretion rate of $200 M_{\odot} \text{ yr}^{-1}$. Given the peculiar distribution of the gas, it is unlikely to be a smooth event. If each of the randomly distributed SGMCS falls into the center separately they will each induce a period of sporadic activity as the gas is assimilated into the central disk. It is hard to believe that under these conditions, the nuclear activity in NGC 985 will not increase significantly – perhaps further increasing the already luminous nature of the AGN.

What might be the effect of this infall on an already active nucleus? One possibility is that some infalling gas will become entrained in a wind presently blowing from the Seyfert core. There is evidence from the X-ray spectrum of a significant soft X-ray component to NGC 985. Some of this may relate to the nuclear star formation which we believe must be present in NGC 985 from the ISO spectral energy distribution, but some may be due to an outflowing wind. It is possible that CO clouds raining towards the center become entrained and accelerated in the outflowing wind and as a result become heated–creating warm outer atmospheres which we tentatively associate with the UV absorption lines and X-ray absorbers. Indeed it would seem natural that inflowing material in tidal interactions involving active nuclei would inevitably encounter winds from the AGN as some stage. This may explain the fact that intrinsic UV absorbers are seen only in a sub-set of cases in UV spectra of Seyfert galaxies (the major accretion stage?). Further observations would be needed to see if the appearance of UV absorbers in AGN spectra is correlated with the appearance of highly asymmetric CO distributions, like that of NGC 985. In any event, our present observations provide for the possibility that the tidal fueling of AGNs must take into account the possibility of potentially complex interactions between the infalling gas and the turn-on of an AGN wind.

The possibility that a nuclear wind could interact, or even disrupt the formation of a central nuclear molecular disk leads to another possible path for the evolution of NGC 985. Could the SGMCS seen in the inner region represent the ending of the ULIRG stage rather than the beginning of it? We have mentioned that many interacting systems show highly concentrated CO disks, and NGC 985 is quite exceptional in that its CO distribution is highly asymmetric–indeed the brighter CO is seen away from the nucleus in the outer disk region, and the CO in the clouds with highly peculiar motions are sig-

nificantly fainter. Could these clouds represent the disrupted remnants of a much more centrally concentrated CO distribution—the stage that is assumed to be associated with ULIRGs?

The question of whether NGC 985 about to become a ULIRG, or alternatively has recently passed through that stage can be tested with future observations. Observations of the elliptical-like bulge component which surrounds the double-nucleus may help to determine whether the galaxy has recently experienced a major episode of global distributed star formation—a symptom of an ongoing or post-merger history (Schweizer 1995). Also, if NGC 985 is emerging, rather than entering a ULIRG stage, it would be expected to show a very extensive soft X-ray emission halo resulting from a recent violent star formation history. High-resolution multi-wavelength IR observations of the bulge may also help to determine what contribution the bulge makes to the strong extended mid-IR emission seen associated with NGC 985. Such observations would help to determine whether the $R^{1/4}$ -law bulge itself contributes a significant amount to the total MIR energy budget of the NGC 985 system.

11. CONCLUSIONS

Observations of NGC 985 with ISO, the VLA and BIMA have led to the following conclusions about this system of galaxies:

1) A MIR luminous AGN is centered on the brighter component of a double nucleus. The MIR nucleus, which is detected in all 4 ISOCAM bands (from $4.5 \mu\text{m}$ to $15 \mu\text{m}$) is consistent with emission from a rapidly rising thermal continuum. The slope of the continuum is consistent with dust heated predominantly by star formation, rather than the AGN itself. We tentatively associate this slightly-extended warm nuclear dust emission with the rapidly rotating stellar and gaseous disk seen at optical wavelengths by Arribas et al. (1999). This disk, which rotates along the line joining the two embedded galactic nuclei, may be forming as a consequence of the merger, resulting from inflowing gas to the nucleus.

2) Our BIMA observations of NGC 985 support the view that it is in a violent state of merger. The CO emission, though covering the nucleus, is distributed in a highly asymmetric distribution, with the peak line-of-sight-column significantly offset from the compact double-nucleus. This distribution resembles the molecular distribution of a number of quasars recently mapped in CO, many of which have asymmetric and irregular CO distributions (Evans et al. 2001). Most of the cool gas in NGC 985 is contained within this large molecular reservoir, which, when adopting standard conversion factors from CO to H_2 masses, contains $1.8 \times 10^{10} M_{\odot}$.

3) Although the highest CO column densities are seen away from the nucleus, we isolate a population of SGMCS which may be mildly collapsing towards the center on a timescale of 60–100 Myrs. These clouds, which extend within 9–10 kpc of the AGN, were identified through their random distribution and unusual motions which are different from the more coherent motions of material further out in the CO ridge. This two-component nature of NGC 985, may indicate a transition time in a merging system in which the motions of the clouds begin to loose

their original ordered motions in the collision, and begin to rain down on the center through dissipation. Sporadic accretion rates are likely to exceed $100 M_{\odot} \text{yr}^{-1}$ if all the molecular material present fall to the center in a few dynamical crossing times.

4) NGC 985 currently has a low ratio of $L_{\text{IR}}/M(\text{H}_2) = 10$. This value lies in the range found for low-luminosity starburst galaxies, despite its abnormal CO distribution and large, as yet mainly untapped, molecular reservoir. This low value may indicate that either i) NGC 985 is about to enter the ULIRG stage as the huge molecular reservoir accumulates at the center, or ii) that the galaxy is emerging from the ULIRG phase, and that the action of a powerful AGN or nuclear starburst wind is inhibiting star formation in the inner regions.

5) We tentatively associate two CO emission features in the direction of the AGN with two out of six narrow UV absorption-lines seen in an HST study of NGC 985. One of these CO emission features is associated with the population of clouds that might be mildly infalling towards the center, and this raises the possibility that the infalling clouds may sometimes become entrained in an outflowing AGN wind. How such interactions may affect the fueling of an AGN over time is not clear. However, these interactions may play an important role in the disruption of centrally concentrated molecular disks in starburst systems that contain powerful AGN.

6) The CO furthest away from the center shows more ordered motions and is associated with the optical/IR ridge—probably a spiral arm or ring-segment containing compressed gas. The tip of the CO ridge, the most distant from the double-nuclei, shows the highest velocity dispersion – a property that seems to correlate with a high rate of local star formation.

7) The ISO observations also reveal warm dust associated with the western optical/IR ridge extending from NGC 985. The dust is consistent with grains heated by bursts of massive star formation which are observed along the ridge and into the outer optical ring of NGC 985. As in the case of the Antennae galaxies, the MIR dust emission does not always scale linearly with other observed properties of the star formation regions (e.g. $\text{H}\alpha$ luminosity, molecular cloud mass). We find that in one region, MIR emission is seen associated with a bright optical H II complex, but no $^{12}\text{CO}(1-0)$ emission is observed at that position, indicating a complicated relationship between dust grain lifetimes and molecular gas lifetimes in massive star formation regions. Our radio continuum observations also provide evidence of a previous episode of star formation which occurred in the recent past inside the ring.

This work was supported in part by NASA grant NAG-5-3317. The authors thank S. Penton and J. Stocke (U. of Colorado) for communicating the results of their HST/STIS study of NGC 985, and for kindly allowing us to present the absorption-line velocities in Table 3 in advance of their publication of the results. We also appreciate the help of A. M. Pérez García and J. M. Rodríguez Espinosa (IAC, Spain) for providing their deep R-band image of NGC 985. P. Appleton would like to thank V. Charmandaris and I. F. Mirabel for their hospitality during the ISO reduction stage of the analysis in France. V. Char-

mandararis would also like to thank O. Laurent (Saclay & MPE) for help and suggestions on the optimum analysis of

ISOCAM data. The authors wish to thank an anonymous referee for helpful comments on the original manuscript.

REFERENCES

- Appleton, P. N., & Marcum, P. M. 1993, *ApJ*, 417, 90
 Appleton, P. N., & Marston A. P. 1997, *AJ*, 113, 201
 Appleton, P. N., & Struck-Marcell, C. 1987, *ApJ*, 318, 103
 Appleton, P. N., & Struck-Marcell, C. 1996, in *Fund. Cosm. Phys.*, 16, 111
 Appleton, P. N., Charmandaris, V., Horellou, C. Mirabel, I.F., Ghigo, F., Higdon, J., & Lord, S. 1999, *ApJ*, 527, 143
 Appleton, P. N., Charmandaris, V., Horellou, C. Mirabel, I.F., & Laurent, O. 2000 in "ISO Surveys of a Dusty Universe", eds. D. Lemke, M. Stickel, K. Wilke, Lecture notes in physics, 548, 231
 Arribas, S., Mediavilla, E., del Burgo, C., García-Lorenzo, B. 1999, *ApJ*, 511, 680
 Bahcall, J. N., & Tremaine, S. 1981, *ApJ*, 244, 805
 Bahcall, J. N., Kirhakos, S., Saxe, D. H., & Schneider, D. P. 1995, *ApJ*, 447, L1
 Bahcall, J. N., Kirhakos, S., Saxe, D. H., & Schneider, D. P. 1997, *ApJ*, 479, 642
 Braine, J., Downes, D., & Guilloteau, S. 1996, *A&A*, 309, L43
 Brandt, W. N., Fabian, A. C., Nandra, K., Reynolds, C. S., & Brinkmann, W. 1994, *MNRAS*, 271, 958
 Bransford, M. A., Appleton, P. N., Marston, A. P., & Charmandaris, V. 1998, *AJ*, 116, 2757
 Bransford, M. A., Appleton, P. N., McCain, C. F., & Freeman, K. C. 1999, *ApJ*, 525, 153
 Cesarsky, C. J., et al. 1996, *A&A*, 315, L32
 Charmandaris, V., Laurent, O., Mirabel, I. F., Gallais, P., Sauvage, M., Vigroux, L., Cesarsky, C., & Appleton, P. N. 1999, *A&A*, 341, 69
 Charmandaris, V., Laurent, O., Mirabel, I. F., Gallais, P., Sauvage, M., Vigroux, L., & Cesarsky, C. 2001, *Ap&SS*, 276, 553
 Clavel, J., et al. 2000, *A&A*, 357, 839
 Condon, J.J., & Yin, Q.F. 1990, *ApJ*, 357, 97
 Coulais, A., & Abergel, A. 2000, *A&AS*, 141, 533
 de Vaucouleurs, G., & de Vaucouleurs, A. 1975, *ApJ*, 197, L1
 Evans, A. S., Kim, D.-C., Mazzarella, J. M., Scoville, N. Z., & Sanders, D. B. 1999, *ApJ*, 521, L107
 Evans, A. S., Frayer, D. T., Surace, J. A., & Sanders, D. B. 2001, *AJ*, 121, 1893
 Frayer, D. T., Brown, R. L., & van den Bout, P. A. 1994, *ApJ*, 433, L5
 Gao, Y., Solomon, P.M., Downes, D., & Radford, S.J.E. 1997, *ApJ*, 481, L35
 Guilloteau, S., Omont, A., Cox, P., McMahan, R. G., & Petitjean, P. 1999, *A&A*, 349, 363
 Heckman, T. M., Balick, B., & Sullivan, W. T. 1978, *ApJ*, 224, 745
 Higdon, J. L., Rand, R. J., & Lord, S. D. 1997, *ApJ*, 489, L133
 Higdon, J. L., Rand, R. J., & Nord, M. 2000, in *American Astronomical Society Meeting*, Vol. 197, 7902
 Högbom, J. A. 1974, *A&A*, 15, 417
 Horellou, C., Casoli, F., Combes, F., & Dupraz, C. 1995, *A&A*, 298, 743
 Horellou, C., Charmandaris, V., Combes, F., Appleton, P. N., Casoli, F., & Mirabel, I. F. 1998, *A&A*, 340, L51
 Jeske, N. A. 1986, Ph. D. Thesis, University of California, Berkeley.
 Kessler, M. F., et al. 1996, *A&A*, 315, L27
 Laurent, O., Mirabel, I. F., Charmandaris, V., Gallais, P., Sauvage, M., Vigroux, L., & Cesarsky, C. 2000, *A&A*, 359, 885
 Le Floch, E., Mirabel, I. F., Laurent, O., Charmandaris, V., Gallais, P., Sauvage, M., Vigroux, L., & Cesarsky, C. 2001, *A&A*, 367, 487
 Limber, D. N., & Mathews, W. G. 1960, *ApJ*, 132, 286
 Lutz, D., Spoon, H. W. W., Rigopoulou, D., Moorwood, A. F. M., Genzel, R. 1998, *ApJ*, 505, L103
 Maiolino, R., Ruiz, M., Rieke, G. H., & Keller, L. D. 1995, *ApJ*, 446, 561
 Mirabel, I. F., & Sanders, D. B. 1989, *ApJ*, 340, L53
 Mirabel, I. F., et al. 1998, *A&A*, 333, L1
 Papadopoulos, P., Ivison, R., Carilli, C., & Lewis, G. 2001, *Nature*, 409, 58
 Pérez García, A. M., & Rodríguez Espinosa, J. M. 1996, *AJ*, 112, 1863
 Rigopoulou, D., Spoon, H. W. W., Genzel, R., Lutz, D., Moorwood, A. F. M., & Tran, Q. D. 1999, *AJ*, 118, 2625
 Rodríguez Espinosa, J. M., & Stanga, R. M. 1990, *ApJ*, 365, 502
 Sanders, D. B., Soifer, B. T., Elias, J. H., Madore, B. F., Matthews, K., Neugebauer, G., & Scoville, N. Z. 1988, *ApJ*, 325, 74
 Sanders, D. B., & Mirabel, I. F. 1996, *ARA&A*, 34, 749
 Schinnerer, E., Eckart, A., & Tacconi, L. J. 1998, *ApJ*, 500, 147
 Schweizer, F. 1995, in "Stellar Populations", IAU Symposium No. 164, Ed. P. C. van der Kruit & G. Gilmore, (Kluwer Academic Publishers, Dordrecht), 275
 Scoville, N. Z., Padin, S., Sanders, D. B., Soifer, B. T., & Yun, M. S. 1993, *ApJ*, 415, L75
 Scoville, N. Z., Yun, M. S., & Bryant, P. M. 1997, *ApJ*, 484, 702
 Skrutskie, M. F., et al. 1997, in "The Impact of Large Scale Near-IR Sky Surveys", eds. F. Garzon et al., (Dordrecht: Kluwer Academic Publishing Company), 25
 Soifer, B. T., Sanders, D. B., Neugebauer, G., Danielson, G. E., Lonsdale, C. J., Madore, B. F., & Persson, S. E. 1986, *ApJ*, 303, L41
 Soifer, B. T., et al. 1999, *ApJ*, 513, 207
 Soifer, B. T., et al. 2001, *AJ*, 122, 1213
 Starck, J.L., Siebenmorgen, R., & Gredel, R. 1997, *ApJ*, 482, 1011
 Stanga, R. M., Rodríguez Espinosa, J. M., & Mannucci, F. 1991, *ApJ*, 379, 592
 Stanford, S. A., Sargent, A. I., Sanders, D. B., & Scoville, N. Z. 1990, *ApJ*, 349, 492
 Stone, O. 1886, *AJ*, 7, 57
 Thronson, H. A., & Greenhouse, M. A. 1984, *ApJ*, 327, 671
 Ulvestad, J. S., & Wilson, A.S. 1984, *ApJ*, 278, 544
 Vigroux, L., et al. 1996, *A&A*, 315, L93
 Welch, W. J., Thornton, D. D., & Plambeck, R. L. 1996, *PASP*, 108, 93
 Wiklind, T., & Combes, F. 1994, *A&A*, 286, L9
 Wilson, C. D., Scoville, N. Z., Madden, S. C., & Charmandaris, V. 2000, *ApJ*, 542, 120
 Young, J. S., & Scoville, N. Z. 1991, *ARA&A*, 29, 581

TABLE 1
RADIO AND MID-INFRARED PROPERTIES OF NGC 985

Region	ISO-LW1 S(4.5 μ m) mJy	ISO-LW7 S(9.7 μ m) mJy	ISO-LW8 S(11.4 μ m) mJy	ISO-LW3 S(15 μ m) mJy	VLA S(3.5 cm) mJy	VLA S(6 cm) mJy
Entire Galaxy	55.2	113.5	154.4	168.9	2.28	4.47
Nucleus/Bulge ^a	46.5	105.6	142.5	163.6	1.49	3.38 ^b
Eastern SF Knot/ring ^c	0.8	5.4	6.2	3.5	0.79	1.09

^aFlux measured in a circular aperture of radius 12 arcsecs centered on the nucleus.

^bUlvestad & Wilson (1984) quote a 6 cm flux for the nucleus of 2.5 mJy with the VLA in A configuration, but mention that this is probably an underestimate of the flux since they note that the flux they detected varied when the array was tapered differently. Our observations, which were made with many short spacings in the D configuration, confirm that the A-array observations missed a substantial fraction of the flux.

^cThe ISO fluxes were evaluated over the bright MIR emission knot centered at $\alpha(\text{J2000}) = 2\text{h } 34\text{m } 36.5\text{s}$, $\delta(\text{J2000}) = -8\text{ d } 47' 10''$, whereas the radio emission was evaluated over the larger area defined by the radio maps of the second western source seen in Fig. 3.

TABLE 2
GLOBAL PROPERTIES OF NGC 985

		Notes
Assumed Distance (Mpc)	170	
m_v (mag)	13.57	: from Appleton & Marston (1997).
L_{IR} (L_{\odot})	1.8×10^{11}	: definition of Sanders & Mirabel (1996).
$M(\text{H I})$ (M_{\odot})	$< 3.6 \times 10^9$: from Heckman et al. (1978) ^a
$S_{\text{CO}} = \int S dv$ (Jy km s^{-1})	54	: from Horellou et al. (1995), filled aperture
$S_{\text{CO}} = \int S dv$ (Jy km s^{-1})	54.8	: (BIMA) this work.
CO Line Width (FWHM, km s^{-1})	408 ± 15	: this work.
$M(\text{H}_2)$ (M_{\odot})	1.8×10^{10}	: this work ^b
$L_{\text{IR}}/M(\text{H}_2)$ (L_{\odot}/M_{\odot})	10	
$M(\text{H}_2)/M(\text{H I})$	> 5.5	

^aBased on Heckman et al. (1978) after correcting for our adopted value of H_0 .

^bUsing a $N(\text{H}_2)/I_{\text{CO}} = 3 \times 10^{20} \text{ mol cm}^{-2} (\text{K km s}^{-1})^{-1}$

TABLE 3
 UV (HST/STIS) OBSERVATIONS OF NUCLEAR ABSORPTION LINES^a

$\text{Ly}\alpha^{\text{b}}$ \AA	Inferred heliocentric cloud velocity km s^{-1}
1264.787 ± 0.02	$12,113 \pm 4$
1265.317 ± 0.02	$12,243 \pm 4$
1265.927 ± 0.06	$12,394 \pm 4$
1266.396 ± 0.05	$12,509 \pm 4$
1267.047 ± 0.02	$12,670 \pm 4$
1268.611 ± 0.00	$13,053 \pm 4$

^aKindly provided by S. Penton & J. Stocke.

^bThe rest wavelength of $\text{Ly}\alpha$ is 1215.67\AA .

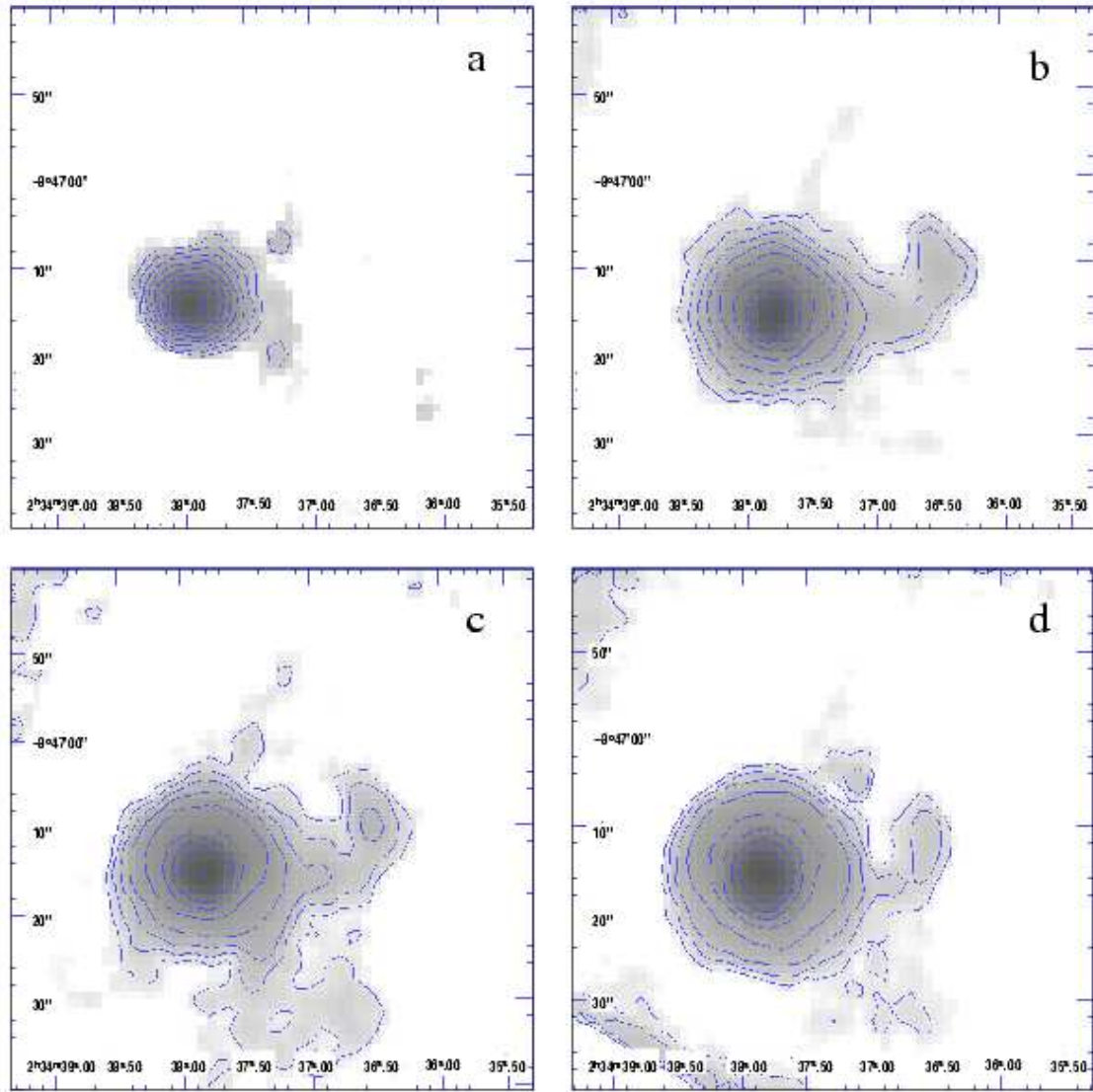


FIG. 1.— a) The ISOCAM $5\ \mu\text{m}$ image of NGC 985, with an overlay of nine of its own contours spanned equally logarithmically between 0.04 and $1.56\ \text{mJy pixel}^{-1}$. The coordinates are in J2000. b-c-d) Same as for a) but for the $9.62\ \mu\text{m}$, $11.4\ \mu\text{m}$, and $15\ \mu\text{m}$ image of the galaxy respectively. The spacing of the nine contours of each image is set as in a) but with limits $[0.02 - 2.47]\ \text{mJy pixel}^{-1}$ for the $9.62\ \mu\text{m}$, $[0.02 - 3.1]\ \text{mJy pixel}^{-1}$ for the $11.4\ \mu\text{m}$ and $[0.02 - 3.4]\ \text{mJy pixel}^{-1}$ for the $15\ \mu\text{m}$ respectively.

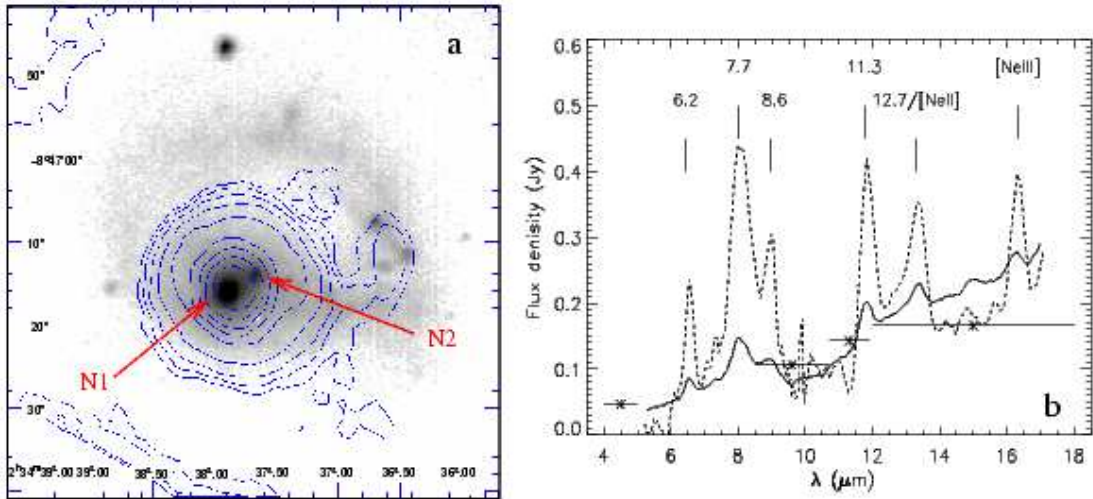


FIG. 2.— a) A contour map of the $15\ \mu\text{m}$ image shown in Fig. 1d) superimposed on an optical R-band image of NGC 985 kindly provided by A. M. Pérez García and J. M. Rodríguez Espinosa (IAC, Spain). The positions of the two nuclei N1 and N2 are marked. b) The nuclear spectrum of NGC 985 as measured with a circular aperture 12 arcsec in radius. The width of each broad-band filter used is marked with a horizontal line. For comparison we display the spectrum of NGC 1068 (from Fig. 3 of Le Floc'h et al. 2001) in solid line, and that of the star forming knot B of the Antennae galaxies (see Vigroux et al. 1996) in dashed line. Both spectra have been red-shifted to the distance of NGC 985 and normalized to the flux density of NGC 985 ISOCAM LW8 ($11.4\ \mu\text{m}$) filter.

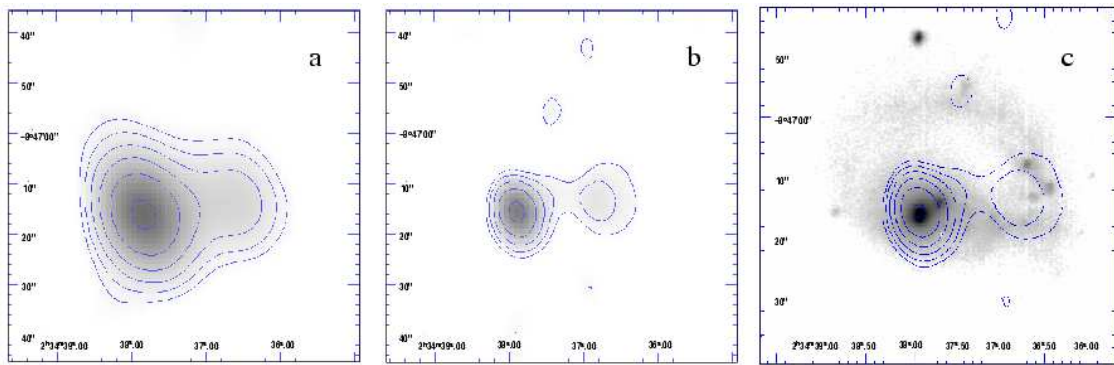


FIG. 3.— a) The VLA 6 cm (C-band) radio continuum map of NGC 985, with an overlay of its own contours. The contours are 0.3, 0.5, 0.8, 1.2, 1.9, and $3.0\ \text{mJy beam}^{-1}$. b) Same in a) but for the 3.5 cm (X-band) radio continuum. The contours are 0.2, 0.3, 0.5, 0.8, 1.3, and $2.0\ \text{mJy beam}^{-1}$. c) Same contours as shown in b) but overlaid on the R-band image of NGC 985 shown in Fig. 2a.

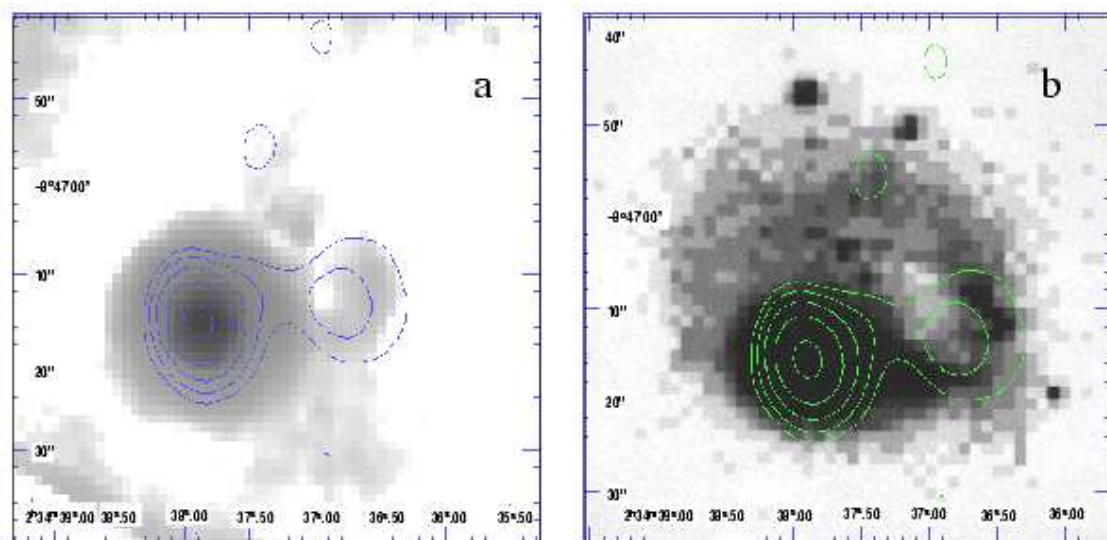


FIG. 4.— a) The 3.5 cm (X-band) contours of NGC 985 overlaid on the $15\ \mu\text{m}$ image of the galaxy. The contour spacing is the same as in Fig 3b. b) Same overlay contours as in a) but this time on the UKIRT K-band image of NGC 985 (see Figures 1 and 2 in Appletton & Marcum 1993).

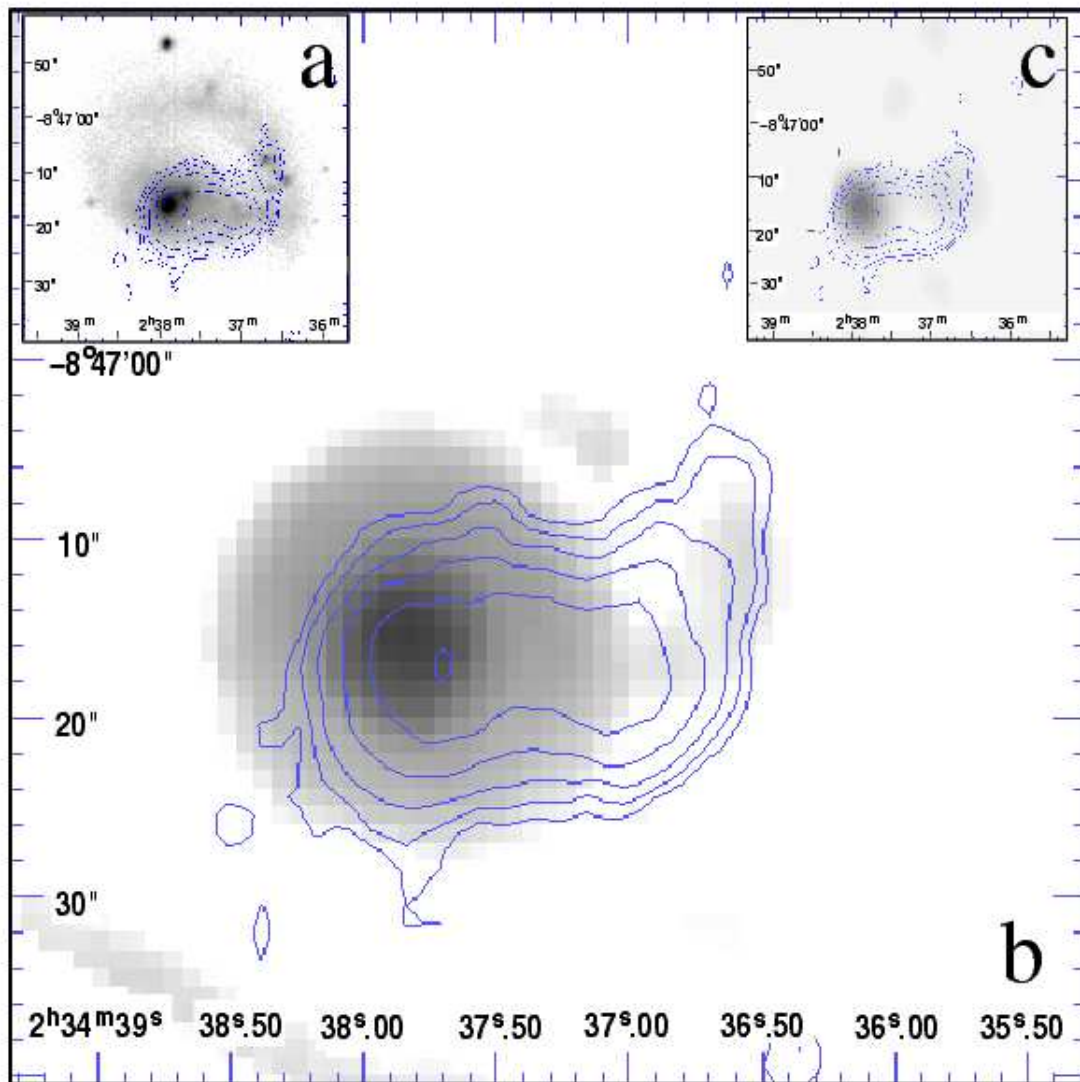


FIG. 5.— a) The integrated $^{12}\text{CO}(1-0)$ emission in contours, over the optical R-band image of NGC 985. The contour levels are 4.0, 5.2, 6.8, 8.8, 11.5 and $15.0 \text{ Jy beam}^{-1} \text{ km s}^{-1}$. b) Same as in a) but the background is the $15 \mu\text{m}$ image of the galaxy. c) Same as in a) but the background is the 3.5 cm (X-band) radio continuum map.

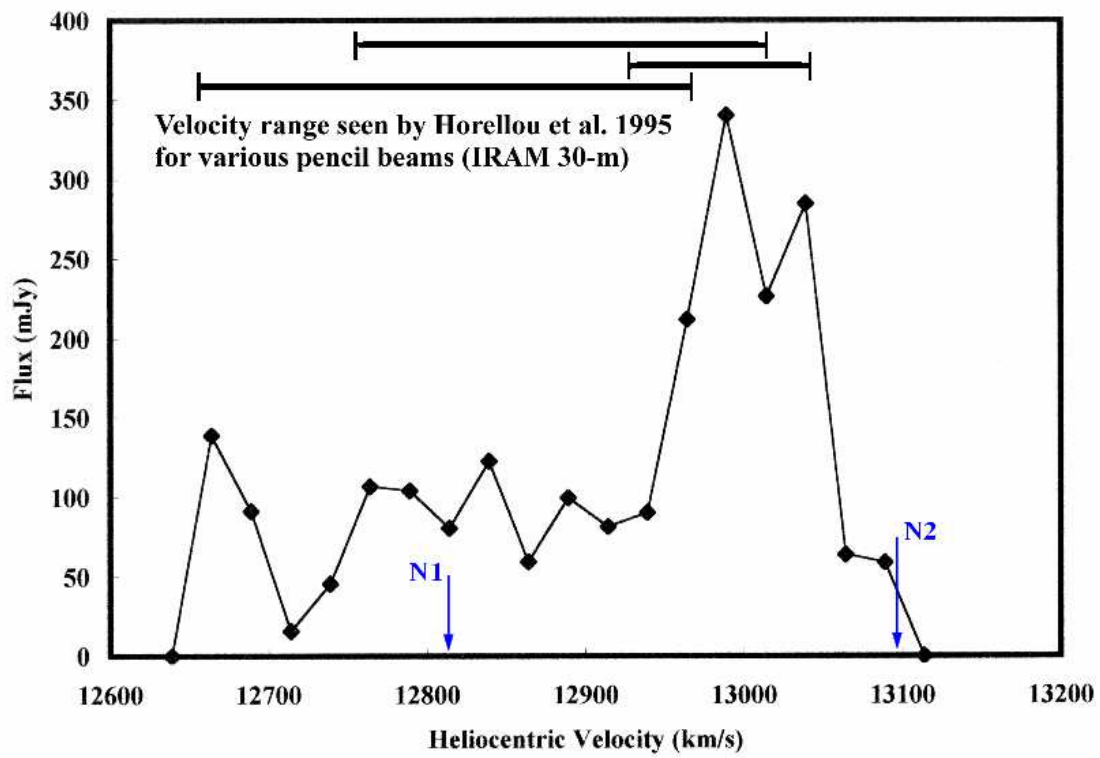


FIG. 6.— Integrated spectrum of the $^{12}\text{CO}(1-0)$ emission from our BIMA data. The optical velocities of the two nuclei, N1 and N2, as well as the velocity ranges seen by the single dish observations of Horellou et al. (1995) are marked.

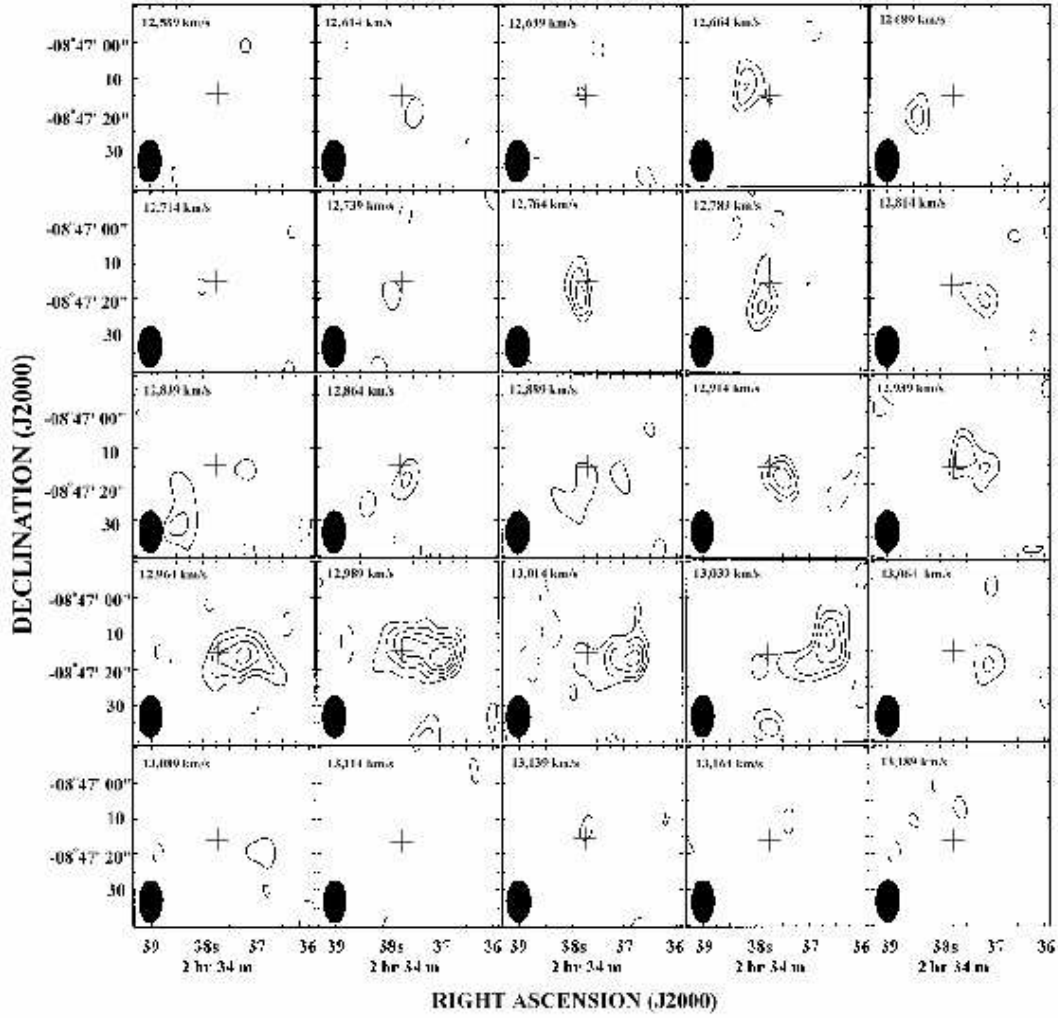


FIG. 7.— Channel maps of the $^{12}\text{CO}(1-0)$ emission from NGC 985. The velocity of each channel is marked on the upper left corner. The contour levels are $n \times 0.015 \text{ Jy beam}^{-1}$ where $n=2,2,3,4,5$, and 6. Negative contours are marked with dashed lines. The first positive contour is close to the 3σ noise level.

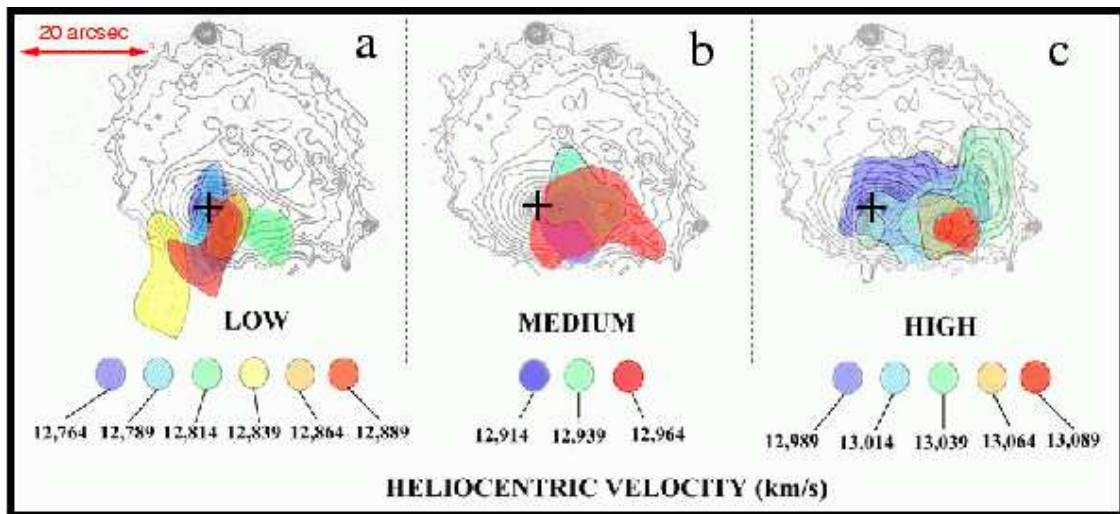


FIG. 8.— A composite of the various emission features superimposed on the K-band UKIRT image of the galaxy. Because the kinematics of the galaxy is unusually complex we have split the figure into three parts, representing the low velocity, medium velocity and high velocity regimes in the data cube (a, b & c respectively). The scale in the upper left corner indicates the angular extent of all the features displayed (see Section 4).

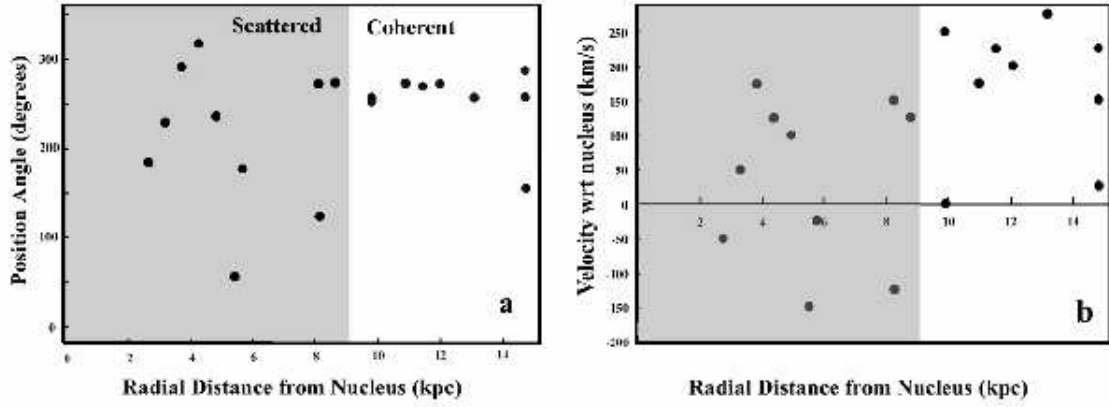


FIG. 9.— a) The position angle as a function of distance from the nucleus N1 of the scattered and coherent SGMCs observed within 15 kpc. b) Same as in a) but plotting the velocity of the SGMCs with respect to N1 as a function of distance. Note how at larger radii the clouds cluster together in one region of each diagram, a result of spatial and kinematic coherence (see discussion in Section 4).

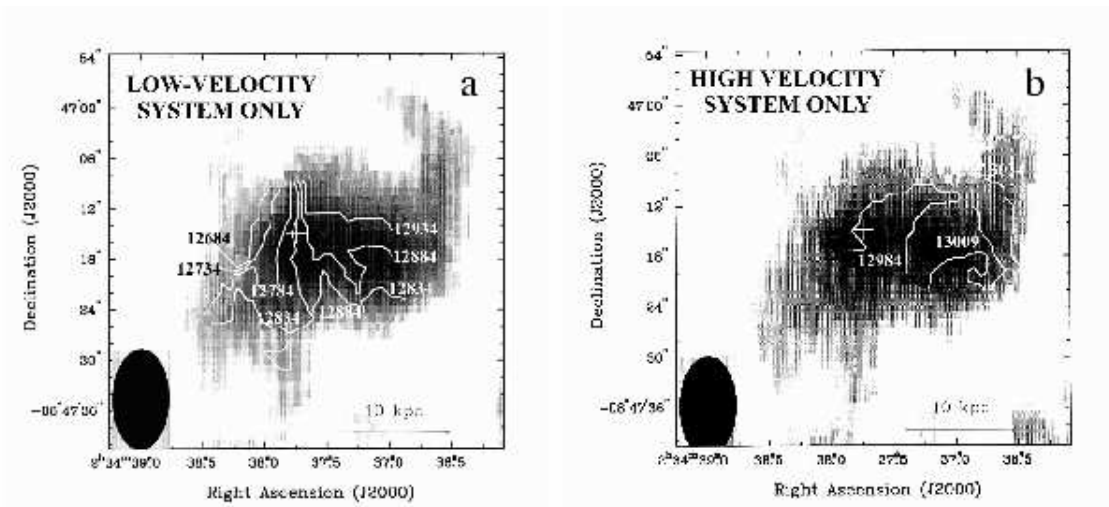


FIG. 10.— a) The isovelocity field of the gas for the low-velocity system superimposed on a grey-scale representation of the CO integrated column density map—heliocentric velocities are in km s^{-1} . b) same as a) but for the high velocity system (see text in Section 4.1).

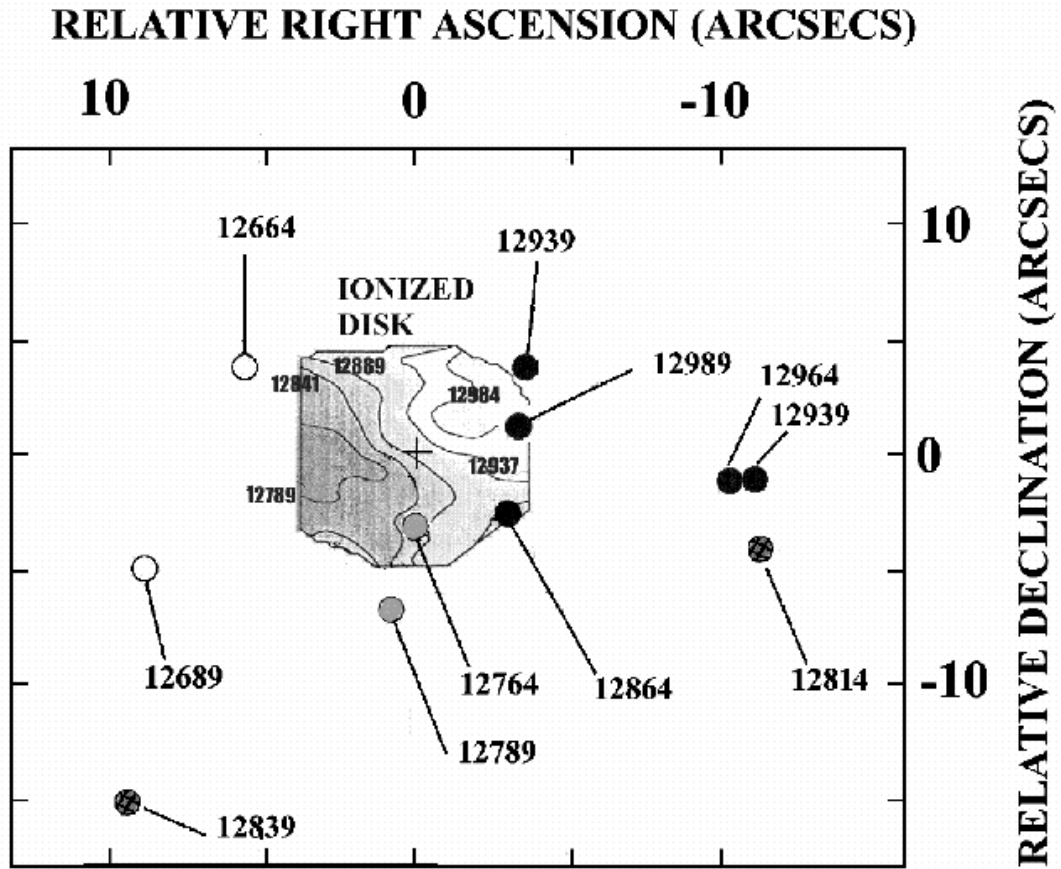


FIG. 11.— Emission centroid positions and velocities for eleven SGMs detected in CO, superimposed on the isovelocity map of the *ionized* gas disk mapped via optical emission lines by Arribas et al. (1999). Note the east-west drift of the CO centroids with increasing velocity and the miss-match with the velocity field of the ionized gas disk (see Section 5).

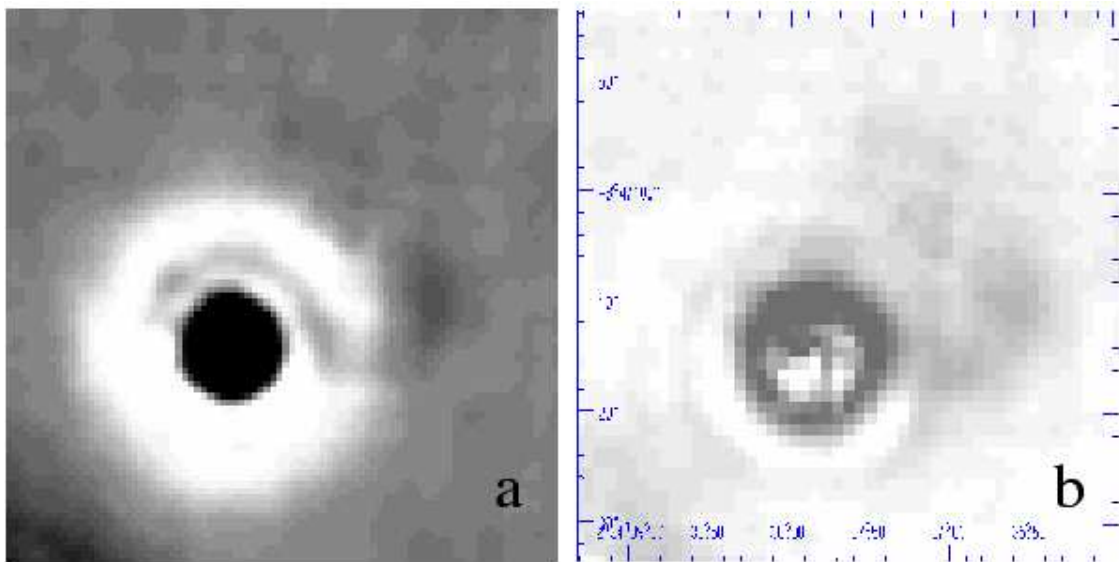


FIG. 12.— a) The $15\ \mu\text{m}$ image of NGC 985 after the unsharp mask technique has been applied. The asymmetric emission and a bright “ridge” to the north and west of the nucleus. b) $15\ \mu\text{m}$ image after a PSF fit and subtraction of the Seyfert nucleus. The field of view is the same as in a). Even though less well defined than the unsharp image one can easily see the same extend in MIR emission to the north of the nucleus.